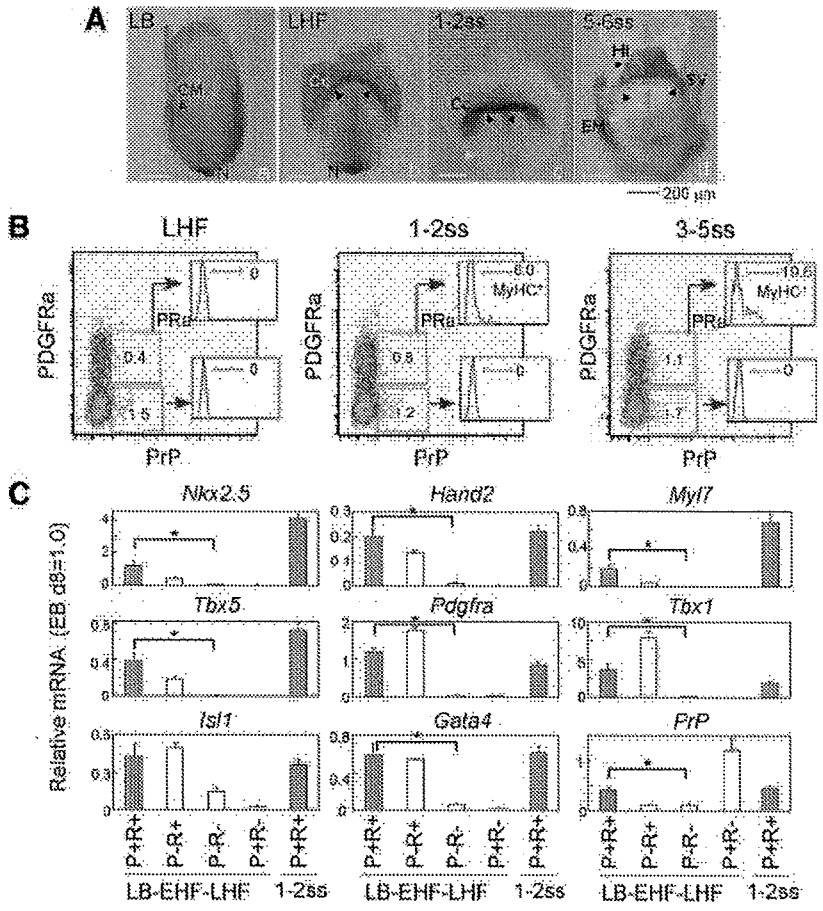

Figure 6. PrP is expressed before Myhc in mouse embryonic cardiac mesoderm. A, Whole-mount in situ hybridization analysis for *Prnp* mRNA (a through c) and immunohistochemical analysis for PrP protein (d). Note that *Prnp* mRNA was expressed in the cardiac mesoderm (CM) beginning at the late-bud stage (LB) and expression was maintained in the cardiac crescent (Cc) and heart tube (Ht) at the late headfold stage (LHF), 1 to 2 somite stage (1 to 2ss), and 3 to 4 somite stage (not shown). PrP was also expressed in the node (N). PrP protein was detected in the cardiac crescent at the late headfold stage (see Online Fig. VI). At the 5- to 6-somite stage, expression was also observed in the sinus venosus (Sv). Nonspecific staining was detected in extraembryonic membrane (EM). B, Flow cytometric analysis of surface and intracellular proteins. After staining the cell surfaces with anti-PrP and anti-PDGFRα antibodies, cells were fixed and permeabilized. Myhc$^+$ cells were first detected in 1- to 2-somite stage embryos and were exclusively observed in the PRa fraction. C, RT-PCR analysis of sorted cells from pools of late-bud to late headfold embryos (LB-EHF-LHF) or 1 to 2 somite embryos (1 to 2 ss). Note that the PRa cell fraction from presomite stages, before Myhc was expressed, was specifically enriched with cardiac markers. Error bars represent the SEMs (n=3 independent samples for each group).

were created from 5000 single-cell isolates (Online Figure III, C). Colony formation was inhibited by the addition of the Wnt inhibitor Dkk1 (dickkopf homolog 1) and promoted by Wnt3a or a glycogen synthase kinase-3β inhibitor, suggesting that the proliferation of PRa cells was dependent on canonical Wnt signaling. Individual colony analysis indicated that approximately 25% of Myhc$^-$ PRa cell–derived colonies expressed both smooth and cardiac muscle proteins (Figure 5C), whereas the rest of the colonies expressed only smooth muscle proteins. Endothelial cell differentiation, assessed based on platelet/endothelial cell adhesion molecule expression, was not observed. These results strongly suggested that the Myhc$^-$ PRa cells contained bipotential (cardiac and smooth muscle) progenitor cells.

Expression of PrP in Mouse Embryos

We next examined the spatial and temporal profiles of PRa cells in embryos. Transgenic mouse studies using β-galactosidase suggested that *Prnp* is expressed in embryonic heart at E8.5.[24] Endogenous expression of PrP mRNA and protein during embryonic early stages (E7 to E7.5) has not been adequately elucidated, however.[25,26] To examine the expression of PrP in early mouse embryos, we performed whole-mount in situ hybridizations and immunohistochemical analysis. During early developmental stages, we observed specific expression of *Prnp* mRNA in the cardiac mesoderm during late-bud stage (Figure 6A). We also detected PrP protein in the cardiac crescent at headfold stages and in the heart tube at somite stages (Online Figure VI). On the other hand, PDGFRα expression was observed widely in the mesoderm, including cardiac mesoderm, of late-bud to 1 to 2 somite stage embryos (Online Figure VI). PDGFRα expression gradually decreased in cardiomyocytes after they reorganized into the heart tube.

We next analyzed PrP expression in mouse embryos using flow cytometry. As expected from the immunohistochemical analysis, PrP$^+$ cells were either PRa cells or PrP$^+$PDGFRα$^-$ cells from the E7 pool (primarily consisting of presomite stage mouse embryos) and the E8 pool (primarily consisting of somite stage mouse embryos) (Online Figure VII, A). As observed in ES cell–derived cells, little overlap between PrP and Flk1 expression was detected at these stages. Sorting using PrP clearly enriched the cardiac marker–expressing cells from the E8 pool (Online Figure VII, B), suggesting that PrP was a specific marker of cardiomyocytes at these stages. To determine whether the PRa population contained both Myhc$^+$ cardiomyocytes and Myhc$^-$ progenitor cells, flow cytometric analysis was performed with embryos at different developmental stages. Myhc$^+$ cells were detected at 1 to 2 somite stages but not at presomite stages. The nascent Myhc$^+$ cells were exclusively identified in the PRa cell

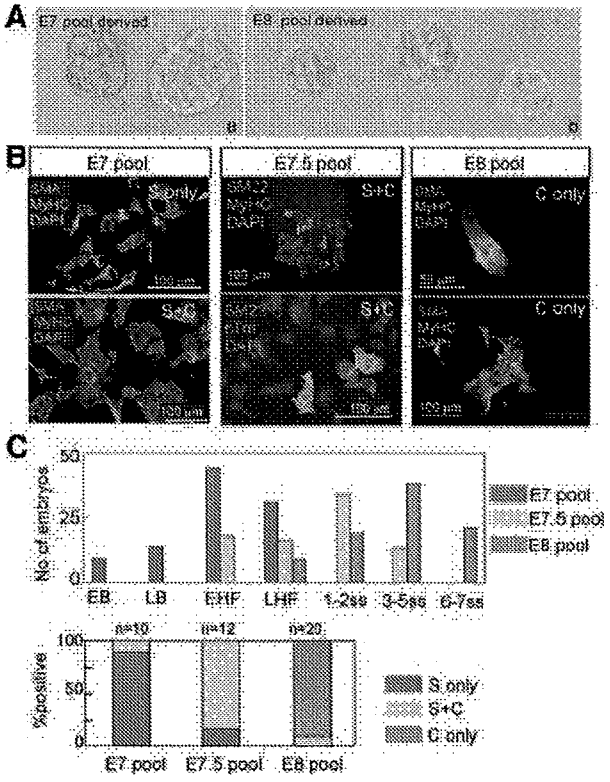

Figure 7. Analysis of single PRa cell–derived colonies from mouse embryos. A, Schematic of the experiment. B, Representative colonies from MEC cultures of E7 pool (a) and E8 pool (b) embryos. Individual colonies from MEC cultures derived from E7 pool, E7.5 pool, or E8 pool embryos were transferred to 96-well plates for immunofluorescence analysis. C, Percentages of the colony types based on immunofluorescence analysis. Embryonic stages in each pool used (top) and colony types derived from each pool (bottom) are shown. The numbers of colonies composed of SMA^+ cells (S only), SMA^+Myhc^+ cells and SMA^+ cells (S+C), or SMA^+Myhc^+ cells (C only) were counted. Eighteen of 20 colonies from the E8 pool contained only cardiomyocytes (C only) and exhibited spontaneous beating.

fraction (Figure 6B). PRa cells sorted from presomite stage embryos (a pool of late-bud to headfold stage embryos) expressed mRNA encoding Nkx2.5, Isl1, Tbx5, and other cardiac transcription factors (Figure 6C). $PrP^+PDGFR\alpha^-$ cells, probably from such extracardiac regions as node, did not express cardiac genes. These results suggested that the embryonic PRa population, similar to ES cell–derived PRa cells, contained $Myhc^+$ nascent cardiomyocytes as well as $Myhc^-$ cardiomyogenic progenitors.

Commitment Status of PRa Cells Derived From Mouse Embryos

We then cultured PRa cells from mouse embryos. Similar to cells from EBs, PRa cells from embryos formed colonies in MEC cultures (Figure 7A). Immunostaining analysis revealed that one of ten colonies derived from an E7 pool contained $Myhc^+$ cells (Figure 7B–C). The other colonies expressed the smooth muscle proteins SMA, SM22, and SMMyhc. PRa cells from the E7.5 pool frequently generated $Mhyc^+$ cardiomyocyte–containing colonies (10 of 12). These samples also contained smooth muscle colonies, suggesting from the presence of bipotential progenitors. PRa cells from the E8 pool generated small beating cardiac colonies. Such beating colonies exclusively contained cardiomyocytes, and not smooth muscle cells, suggesting that the isolated cells were committed to the cardiomyogenic lineage. These results suggested that PRa cells isolated from the cardiac mesoderm could differentiate into either cardiac or smooth muscle cells. Thus, PRa cells from mouse embryos and EBs may share common differentiation and proliferation potentials.

Discussion

In this study, we have demonstrated that the surface marker PrP can be used to enrich cardiomyocytes derived from ES cells. Several groups have examined methods to enrich cardiomyocytes using gravity or introduction of a selectable marker. Surface markers that allow cardiomyocytes to be selected directly, however, have not been extensively elucidated. Importantly, up to 90% of cells derived from PrP^+ cell cultures expressed cTnI (a marker for definitive cardiomyocytes). The other cells expressed SMA, suggesting that the cultures contained at least 2 different lineages. To improve the purity of the population, other markers or directional differentiation methods should be combined with PrP expression. We also showed that the cultured PrP^+ cells differentiated into both atrial and ventricle cardiomyocytes. Hcn4 protein, a specific marker for sinus node, was barely detectable. Because spontaneous pacemaker-like activity was detected in immature atrial or ventricular cardiomyocytes, PrP^+ cells may not have differentiated into mature sinus node cells, at least under our culture conditions. Cells expressing ANP, a marker of chamber myocardium,[27] were not found in significant numbers in the PrP^+ cell cultures, suggesting that the PrP^+ cells had not differentiated into chamber myocardium cells. Consistent with this idea, flow cytometric analysis of the expression patterns of Mylc2v and ANP produced results that were more similar to those observed for E9.5 heart than for E13.5 heart.

At earlier stages, PrP did not define a cardiomyogenic population. The $PrP^+PFGFR\alpha^+$ fraction (PRa cells) contained nascent cardiomyocytes and their progenitors. It would be interesting to understand the relationship between PRa cells and previously described cardiovascular progenitor/stem cells. Because PRa cells did not markedly express Flk1, they may have segregated from the endothelial lineage. Consistent with this idea, we did not observe endothelial cell differentiation from PRa cell–derived cells even in the OP9 culture system, which efficiently supported endothelial cell differentiation (Online Figure V). The proliferation and differentiation of PRa cells are regulated positively and negatively by Wnt signals, respectively. The presence of $Isl1^+$ cells in the PRa cell population (Online Figure IV, E) indicates that PRa cells represent an intermediate progenitor, located between $Isl1^+$ multipotential cells and committed cardiomyocytes. Other groups have described bipotential progenitors, such as $c\text{-}kit^+Nkx2.5^+$ cells and $Tbx18^+$ epicardial cells.[28,29] Because PRa cells did not display surface expression of c-kit,

they are likely not related to c-kit$^+$Nkx2.5$^+$ cells. Interestingly, we observed Tbx18 expression in PRa cell–derived 2D cultures but not in 3D cultures (data not shown). Recent studies showed that the Nkx2.5$^+$ lineage also diverges into Tbx18$^+$ epicardial cells.[30] Thus, it would be intriguing to know if PRa cells can differentiate into epicardial cells.

Embryonic localization in the cardiac crescent and their limited differentiation potential strongly suggest that PRa cells include progenitors from the primary heart field. Consistent with this idea, PRa cells sorted from presomite-stage embryos expressed Tbx5. On the other hand, PRa cells also include progenitors from the secondary heart field, because they also expressed Tbx1 and Isl1. Flow cytometric analysis further revealed that PRa cells were present in the outflow tract segment, which is derived from the secondary lineage (Online Figure VII, C). As in the early somite stages, outflow-derived PRa cells included Myhc$^+$ cells. Thus, PRa can serve as a pan-marker for cardiomyogenic progenitors independent of the heart field lineage. Interestingly, compared with embryo-derived PRa cells, EB-derived PRa cells expressed lower levels of Tbx1. This suggests that, under our culture conditions, primary heart lineage progenitors preferentially developed. However, it should be determined whether or not EB-derived PRa cells differentiated into outflow cardiomyocytes.

Based on molecular studies and in vitro cultures of isolated cells, we propose that PRa cells include a cardiomyogenic population, which can differentiate into cardiac or smooth muscle cells (Online Figure VIII). Considering their limited differentiation potential, PRa cells may be downstream of Flk1$^+$ cells, separate from the endothelial lineage. Immediate early progenitors may be in the Flk1$^+$PDGFRα^+ fraction, because this transient cell faction (observed on day 5) specifically expressed *Mesp1* (data not shown). Multipotent or pluripotent stem cells, including induced pluripotent stem cells, are expected to be a powerful tool for transplantation therapy and drug screening. Testing the ability of ES cell–derived cardiomyocytes to rescue in vivo heart function has been hampered by a lack of markers that allow scalable purification of the population without recourse to the genetic manipulations required to insert lineage- or stage-specific selectable markers. The mouse cell surface marker PrP defines a cardiogenic population in differentiating ES cells, enabling efficient isolation and enrichment of ES cell–derived cardiomyocytes.

Acknowledgments

We thank S. Suzuki, M. Honda, and other members of the Morisaki laboratory for technical assistance.

Sources of Funding

This work was supported, in part, by the National Institute of Biomedical Innovation (NIBIO); the Ministry of Health, Labour and Welfare; and the Ministry of Education, Culture, Sports, Science and Technology, Japan (K. H. and T. M.). M. D. S. is the British Heart Foundation Simon Marks Chair in Regenerative Cardiology.

Disclosures

None.

References

1. Brand T. Heart development: molecular insights into cardiac specification and early morphogenesis. *Dev Biol.* 2003;258:1–19.
2. Buckingham M, Meilhac S, Zaffran S. Building the mammalian heart from two sources of myocardial cells. *Nat Rev Genet.* 2005;6:826–835.
3. Laugwitz KL, Moretti A, Caron L, Nakano A, Chien KR. Islet1 cardiovascular progenitors: a single source for heart lineages? *Development.* 2008;135:193–205.
4. Hochgreb T, Linhares VL, Menezes DC, Sampaio AC, Yan CY, Cardoso WV, Rosenthal N, Xavier-Neto J. A caudorostral wave of RALDH2 conveys anteroposterior information to the cardiac field. *Development.* 2003;130:5363–5374.
5. Kattman SJ, Huber TL, Keller GM. Multipotent flk-1+ cardiovascular progenitor cells give rise to the cardiomyocyte, endothelial, and vascular smooth muscle lineages. *Dev Cell.* 2006;11:723–732.
6. Yamaguchi TP, Dumont DJ, Conlon RA, Breitman ML, Rossant J. flk-1, an flt-related receptor tyrosine kinase is an early marker for endothelial cell precursors. *Development.* 1993;118:489–498.
7. Moretti A, Caron L, Nakano A, Lam JT, Bernshausen A, Chen Y, Qyang Y, Bu L, Sasaki M, Martin-Puig S, Sun Y, Evans SM, Laugwitz KL, Chien KR. Multipotent embryonic isl1+ progenitor cells lead to cardiac, smooth muscle, and endothelial cell diversification. *Cell.* 2006;127:1151–1165.
8. Wu SM, Fujiwara Y, Cibulsky SM, Clapham DE, Lien CL, Schultheiss TM, Orkin SH. Developmental origin of a bipotential myocardial and smooth muscle cell precursor in the mammalian heart. *Cell.* 2006;127:1137–1150.
9. Kwon C, Arnold J, Hsiao EC, Taketo MM, Conklin BR, Srivastava D. Canonical Wnt signaling is a positive regulator of mammalian cardiac progenitors. *Proc Natl Acad Sci U S A.* 2007;104:10894–10899.
10. Naito AT, Shiojima I, Akazawa H, Hidaka K, Morisaki T, Kikuchi A, Komuro I. Developmental stage-specific biphasic roles of Wnt/beta-catenin signaling in cardiomyogenesis and hematopoiesis. *Proc Natl Acad Sci U S A.* 2006;103:19812–19817.
11. Nakamura T, Sano M, Songyang Z, Schneider MD. A Wnt- and beta-catenin-dependent pathway for mammalian cardiac myogenesis. *Proc Natl Acad Sci U S A.* 2003;100:5834–5839.
12. Ueno S, Weidinger G, Osugi T, Kohn AD, Golob JL, Pabon L, Reinecke H, Moon RT, Murry CE. Biphasic role for Wnt/beta-catenin signaling in cardiac specification in zebrafish and embryonic stem cells. *Proc Natl Acad Sci U S A.* 2007;104:9685–9690.
13. Laflamme MA, Chen KY, Naumova AV, Muskheli V, Fugate JA, Dupras SK, Reinecke H, Xu C, Hassanipour M, Police S, O'Sullivan C, Collins L, Chen Y, Minami E, Gill EA, Ueno S, Yuan C, Gold J, Murry CE. Cardiomyocytes derived from human embryonic stem cells in pro-survival factors enhance function of infarcted rat hearts. *Nat Biotechnol.* 2007;25:1015–1024.
14. van Laake LW, Passier R, Doevendans PA, Mummery CL. Human embryonic stem cell-derived cardiomyocytes and cardiac repair in rodents. *Circ Res.* 2008;102:1008–1010.
15. Nelson TJ, Faustino RS, Chiriac A, Crespo-Diaz R, Behfar A, Terzic A. CXCR4+/FLK-1+ biomarkers select a cardiopoietic lineage from embryonic stem cells. *Stem Cells.* 2008;26:1464–1473.
16. Liu Y, Asakura M, Inoue H, Nakamura T, Sano M, Niu Z, Chen M, Schwartz RJ, Schneider MD. Sox17 is essential for the specification of cardiac mesoderm in embryonic stem cells. *Proc Natl Acad Sci U S A.* 2007;104:3859–3864.
17. Terami H, Hidaka K, Shirai M, Narumiya H, Kuroyanagi T, Arai Y, Aburatani H, Morisaki T. Efficient capture of cardiogenesis-associated genes expressed in ES cells. *Biochem Biophys Res Commun.* 2007;355:47–53.
18. Linden R, Martins VR, Prado MA, Cammarota M, Izquierdo I, Brentani RR. Physiology of the prion protein. *Physiol Rev.* 2008;88:673–728.
19. Zhang CC, Steele AD, Lindquist S, Lodish HF. Prion protein is expressed on long-term repopulating hematopoietic stem cells and is important for their self-renewal. *Proc Natl Acad Sci U S A.* 2006;103:2184–2189.
20. Hidaka K, Lee JK, Kim HS, Ihm CH, Iio A, Ogawa M, Nishikawa S, Kodama I, Morisaki T. Chamber-specific differentiation of Nkx2.5-positive cardiac precursor cells from murine embryonic stem cells. *FASEB J.* 2003;17:740–742.
21. Kouskoff V, Lacaud G, Schwantz S, Fehling HJ, Keller G. Sequential development of hematopoietic and cardiac mesoderm during embryonic stem cell differentiation. *Proc Natl Acad Sci U S A.* 2005;102:13170–13175.

22. Westfall MV, Samuelson LC, Metzger JM. Troponin I isoform expression is developmentally regulated in differentiating embryonic stem cell-derived cardiac myocytes. *Dev Dyn.* 1996;206:24–38.
23. Prall OW, Menon MK, Solloway MJ, Watanabe Y, Zaffran S, Bajolle F, Biben C, McBride JJ, Robertson BR, Chaulet H, Stennard FA, Wise N, Schaft D, Wolstein O, Furtado MB, Shiratori H, Chien KR, Hamada H, Black BL, Saga Y, Robertson EJ, Buckingham ME, Harvey RP. An Nkx2–5/Bmp2/Smad1 negative feedback loop controls heart progenitor specification and proliferation. *Cell.* 2007;128:947–959.
24. Tremblay P, Bouzamondo-Bernstein E, Heinrich C, Prusiner SB, DeArmond SJ. Developmental expression of PrP in the post-implantation embryo. *Brain Res.* 2007;1139:60–67.
25. Bosque PJ, Ryou C, Telling G, Peretz D, Legname G, DeArmond SJ, Prusiner SB. Prions in skeletal muscle. *Proc Natl Acad Sci U S A.* 2002; 99:3812–3817.
26. Manson J, West JD, Thomson V, McBride P, Kaufman MH, Hope J. The prion protein gene: a role in mouse embryogenesis? *Development.* 1992;115:117–122.
27. Christoffels VM, Habets PE, Franco D, Campione M, de Jong F, Lamers WH, Bao ZZ, Palmer S, Biben C, Harvey RP, Moorman AF. Chamber formation and morphogenesis in the developing mammalian heart. *Dev Biol.* 2000;223:266–278.
28. Cai CL, Martin JC, Sun Y, Cui L, Wang L, Ouyang K, Yang L, Bu L, Liang X, Zhang X, Stallcup WB, Denton CP, McCulloch A, Chen J, Evans SM. A myocardial lineage derives from Tbx18 epicardial cells. *Nature.* 2008;454:104–108.
29. Christoffels VM, Grieskamp T, Norden J, Mommersteeg MT, Rudat C, Kispert A. Tbx18 and the fate of epicardial progenitors. *Nature.* 2009; 458:E8–E9.
30. van Wijk B, van den Berg G, Abu-Issa R, Barnett P, van der Velden S, Schmidt M, Ruijter JM, Kirby ML, Moorman AF, van den Hoff MJ. Epicardium and myocardium separate from a common precursor pool by crosstalk between bone morphogenetic protein- and fibroblast growth factor-signaling pathways. *Circ Res.* 2009;105:431–441.

Nongenetic method for purifying stem cell–derived cardiomyocytes

Fumiyuki Hattori[1,2], Hao Chen[1,3], Hiromi Yamashita[1], Shugo Tohyama[1,3], Yu-suke Satoh[1,4], Shinsuke Yuasa[1], Weizhen Li[1], Hiroyuki Yamakawa[1,3], Tomofumi Tanaka[1,2], Takeshi Onitsuka[1,3], Kenichiro Shimoji[1,3], Yohei Ohno[1,3], Toru Egashira[1,3], Ruri Kaneda[1], Mitsushige Murata[1,3], Kyoko Hidaka[5], Takayuki Morisaki[5], Erika Sasaki[6], Takeshi Suzuki[4], Motoaki Sano[1], Shinji Makino[1], Shinzo Oikawa[2] & Keiichi Fukuda[1]

Several applications of pluripotent stem cell (PSC)-derived cardiomyocytes require elimination of undifferentiated cells. A major limitation for cardiomyocyte purification is the lack of easy and specific cell marking techniques. We found that a fluorescent dye that labels mitochondria, tetramethylrhodamine methyl ester perchlorate, could be used to selectively mark embryonic and neonatal rat cardiomyocytes, as well as mouse, marmoset and human PSC-derived cardiomyocytes, and that the cells could subsequently be enriched (>99% purity) by fluorescence-activated cell sorting. Purified cardiomyocytes transplanted into testes did not induce teratoma formation. Moreover, aggregate formation of PSC-derived cardiomyocytes through homophilic cell-cell adhesion improved their survival in the immunodeficient mouse heart. Our approaches will aid in the future success of using PSC-derived cardiomyocytes for basic and clinical applications.

Human embryonic stem cells (ESCs) and induced pluripotent stem cells (iPSCs) could prove to be an unlimited source of cardiomyocytes. Several studies have achieved directed differentiation of mouse, monkey and human ESCs into cardiomyocytes[1–3] but with variable efficiency. Some protocols describe up to 60% differentiation efficiency, but none achieve >99% of cells differentiating into cardiomyocytes without the use of genetic selection methods[4]. Transplantation of undifferentiated ESCs results in the formation of teratomas[5]. Thus, it is necessary to purify ESC-derived cardiomyocytes before transplantation.

ESC lines with various combinations of cardiomyocyte-specific reporters can be used to obtain highly pure ESC-derived cardiomyocytes[4,6–10], but this requires genetic modification of the cells. Also, discontinuous Percoll density gradient centrifugation could be used to enrich for mouse and human ESC-derived cardiomyocytes, but the purity of the cardiomyocytes in these preparations is relatively low[11,12]. Here we show that cardiomyocytes in early mouse embryos or those differentiated from pluripotent stem cells (PSCs) have high mitochondrial content and can be purified without the need for genetic modification, using fluorescent dyes that label mitochondria.

RESULTS

Characterization of mitochondrial dyes

In primary cultures of neonatal rat heart cells stained with MitoTracker Red (Invitrogen) the fluorescence intensity of cardiomyocytes was much higher compared to that of non-myocytes (**Fig. 1a**). MitoTracker Red and tetramethylrhodamine methyl ester perchlorate (TMRM) specifically accumulated in both the subsarcomeric mitochondria, located around the nucleus and in the intermyofibrillar mitochondria (**Fig. 1a** and **Supplementary Fig. 1**). To confirm specific mitochondrial staining of MitoTracker dyes, we stained neonatal rat cardiomyocytes with MitoTracker Red and JC-1 (a mitochondrial voltage-sensitive dye; **Supplementary Fig. 2**).

Fluorescence-activated cell sorter (FACS) analysis of cells dissociated from neonatal heart revealed three main populations (**Fig. 1b**). We sorted the populations with the highest (designated as fraction 1), the middle (fraction 2) and the lowest (fraction 3) fluorescence intensity and cultured them separately. All the cells in fraction 1 showed rhythmic beating and were immunostained with an antibody to α-actinin (**Fig. 1c**), indicating they were cardiomyocytes. We identified very few cardiomyocytes in fraction 2 (**Fig. 1c**). Fraction 3 consisted of red blood cells and dead cells. We confirmed the neonatal rat cardiomyocyte content in fraction 1 by immunofluorescence staining for α-actinin to be 99.4 ± 0.6% (**Fig. 1d**), and the yield was approximately 5×10^5 cells from a single heart.

Next, we compared the efficacy of various mitochondrial dyes for separating the neonatal rat cardiomyocyte population from the nonmyocytes and found that TMRM was the most effective (**Fig. 1e,f**). We then evaluated the washout efficiencies of the dyes and found that TMRM disappeared completely within 24 h, whereas

[1]Department of Regenerative Medicine and Advanced Cardiac Therapeutics, Keio University School of Medicine, Tokyo, Japan. [2]Asubio Pharma Co., Ltd., Osaka, Japan. [3]Division of Cardiology, Department of Medicine, Keio University School of Medicine, Tokyo, Japan. [4]Division of Basic Biological Sciences, Faculty of Pharmacy, Keio University, Tokyo, Japan. [5]Department of Bioscience, National Cardiovascular Center Research Institute, Osaka, Japan. [6]Laboratory of Applied Developmental Biology, Marmoset Research Department, Central Institute for Experimental Animals, Kanagawa, Japan. Correspondence should be addressed to K.F. (kfukuda@sc.itc.keio.ac.jp).

RECEIVED 10 AUGUST; ACCEPTED 15 OCTOBER; PUBLISHED ONLINE 29 NOVEMBER 2009; DOI:10.1038/NMETH.1403

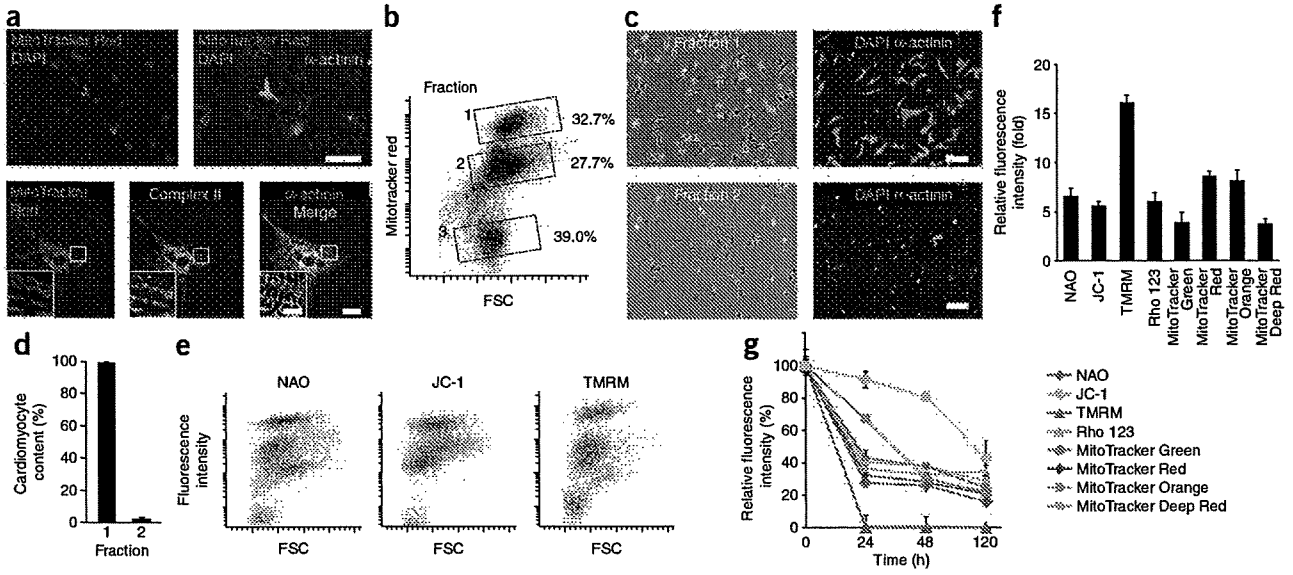

Figure 1 | Mitochondrial dyes for cardiomyocyte purification. (**a**) Fluorescence images of neonatal rat cardiomyocytes prestained with MitoTracker Red and immunostained for α-actinin (top) or prestained with MitoTracker Red and immunostained for mitochondrial electron transfer chain complex II (complex II) and α-actinin (bottom). DAPI, nuclear stain. Scale bars, 100 μm (top); 20 μm (bottom); and 10 μm (bottom inset). (**b**) FACS analysis of neonatal rat heart–derived cells stained with MitoTracker Red. The sorted cells were divided into fractions 1–3 (boxed). FSC, forward scatter. (**c**) Immunofluorescence staining for α-actinin of cells from fractions 1 and 2. Blue, DAPI staining. Scale bars, 100 μm. (**d**) Cardiomyocyte content in fractions 1 and 2. Data are shown as mean ± s.d. (n = 3). (**e**) Representative FACS plots of dissociated cells from neonatal rat heart stained with mitochondrial dyes. (**f**) Relative fluorescence intensity of the indicated mitochondrial dyes in fractions 1 versus 2. Data are shown as mean ± s.d. (n = 3). (**g**) Washout of the indicated mitochondrial dyes from neonatal rat cardiomyocytes. Data are shown as mean ± s.d. (n = 3).

other dyes remained for at least 5 d (**Fig. 1g** and **Supplementary Fig. 3a**). TMRM and JC-1 at 100 nM did not affect cell viability using 3-(4,5-dimethyl-thiazol-2-yl)-2,5-diphenyltetrazolium bromide (MTT) assay, whereas other dyes affected viability differently (**Supplementary Fig. 3b**). Based on these results, we selected TMRM for subsequent experiments.

Purification of cardiomyocytes from heart and whole embryos

To investigate the mitochondrial content of cardiomyocytes at different developmental stages, we performed FACS analysis of rat hearts at embryonic day 11.5 (E11.5) to postnatal day 8 (P8); the hearts had been dissociated and labeled with TMRM (**Fig. 2a**). The mean ratio of TMRM fluorescence in fraction 1 to fraction 2 gradually increased with increasing embryonic stage and rapidly after birth (**Fig. 2b**). FACS analysis followed by immunofluorescence staining confirmed over 99% cardiomyocyte purity at all stages (**Fig. 2c,d**).

We then stained live embryos (E11.5 and E12.5) with TMRM. The heart showed markedly stronger fluorescence compared with other tissues (**Fig. 2e** and **Supplementary Video 1**). Intraplacental injection of MitoTracker Red also resulted in the strongest accumulation of fluorescence in the heart via embryonic circulation. However, other tissues had much weaker fluorescence (**Supplementary Fig. 4**).

To assess why there was strong TMRM fluorescence in the embryonic heart, we compared expression levels of complex I–V of the 36 kDa mitochondrial outer membrane protein porin (also known as the voltage-dependent anion channel) and of heat shock protein 70 between cardiac and various noncardiac tissues in rat E12.5 embryos; we detected markedly stronger expression in the myocardium (**Supplementary Fig. 5**). Furthermore, immunostaining of the fetal heart area for α-actinin, manganese superoxide dismutase (MnSOD) and platelet endothelial cell adhesion molecule (PECAM) (markers of cardiomyocytes, mitochondria and the endothelium, respectively), revealed that MnSOD immunostaining overlapped that for α-actinin but not for PECAM (**Fig. 2f**). Taken together, the accumulation of fluorescent dyes that label mitochondria may reflect high mitochondria abundance in the heart.

Next, we treated dissociated cells obtained from E11.5 to E13.5 whole rat embryos with TMRM and analyzed them on a FACS (**Fig. 2g**). Some cells in this preparation were autofluorescent, which was due to the presence of lipopigments and flavins[13]. To obtain only TMRM-fluorescent cells and eliminate contamination by autofluorescent cells, we adopted pseudo-two-dimensional separation (**Fig. 2g** and Online Methods). We isolated populations with the highest TMRM-fluorescence from dispersed cells of E11.5, E12.5 and E13.5 whole rat embryos. The sorted cells from E11.5 embryos were immunostained for α-actinin (purity 99%, n = 3 embryos; yield, ~5 × 10^3 cells per embryo). We obtained similar results with E12.5 and E13.5 embryos. At these embryonic stages (E11.5–E13.5), the embryos contain skeletal myoblasts only and not mature myotubes. We found that mature skeletal myotubes, which could not pass through the FACS, could be marked with TMRM, whereas skeletal myoblasts, which do pass through the FACS, were not marked by TMRM (**Supplementary Fig. 6**).

Purification of PSC-derived cardiomyocytes

We first observed cardiomyocytes differentiated from mouse ESCs on day 7 of differentiation; the cells had marked TMRM accumulation. After TMRM staining, we fixed the cells and immunostained them for Nkx2.5 and α-actinin (**Fig. 3a**). The Nkx2.5– and α-actinin–positive areas and TMRM-positive area in the mouse

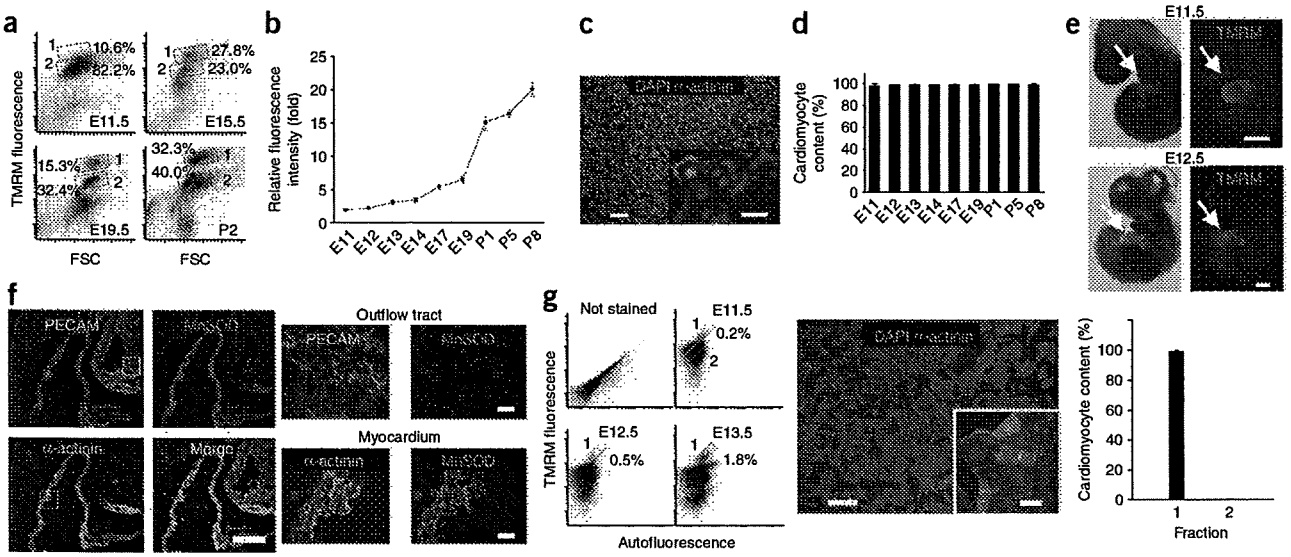

Figure 2 | Purification of cardiomyocytes from embryonic heart and whole embryo. (**a**) Representative FACS analysis of TMRM-stained rat embryonic heart cells at the indicated ages. Fractions 1 and 2 were typical gates for cardiomyocytes and noncardiomyocytes, respectively. (**b**) Relative fluorescence intensity of fraction 1 versus fraction 2 in the developing rat heart. Data are shown as mean ± s.d. ($n = 3$). (**c**) Immunofluorescence staining for α-actinin in the fraction 1 gated cells from E11.5 rat heart. (**d**) Cardiomyocyte content of the fraction 1-gated cells obtained from E11.5–P8 rat hearts. Data are shown as mean ± s.d. ($n = 3$). (**e**) Bright field (left) and fluorescence (right) images of whole rat embryos of indicated ages. (**f**) Immunofluorescence staining of rat E11.5 embryo for the indicated markers, PECAM, α-actinin and MnSOD. Images show pericardiac area (left four) and magnification of the boxed areas is shown on the right. (**g**) FACS analysis (left) of dissociated cells from whole embryos in the absence (not stained) or presence of TMRM at the indicated stages. Boxes indicate fractions 1 and 2; percentages of fraction 1 cells are shown. Immunofluorescence staining (middle) for α-actinin in the cells obtained from fraction 1 of E11.5 embryos. Cardiomyocyte content of fractions 1 and 2 at E11.5 is shown (right). Data are shown as mean ± s.d. ($n = 3$). Scale bars, 100 μm (**c**,**g**,**e**); 200 μm (**f** left); and 20 μm (**c** inset, **f** right, **g** inset).

ESC–derived cardiomyocytes were colocalized completely, although the intracellular localization of TMRM, Nkx2.5 and α-actinin was clearly different. Notably, TMRM dissociated rapidly into the bulk solution compared with other dyes upon fixation (**Supplementary Fig. 7**), indicating that there is likely to be no effect of TMRM on subsequent immunohistochemical analysis.

We applied pseudo–two-dimensional FACS analysis to the embryoid body–derived cells (**Fig. 3b**). We first observed fraction 1 cells 7 d after embryoid body formation. Both the ratio of the mean TMRM fluorescence in fraction 1 (cardiomyocytes) to fraction 2 (noncardiomyocytes) and the percentage of cells in fraction 1 increased gradually until day 15 (**Fig. 3c,d**), suggesting that the best time for obtaining mouse ESC–derived cardiomyocytes was at day 15.

We sorted approximately 5×10^5 to 9×10^5 cells from day 15 embryoid bodies. The viability of the sorted cells was 99.1 ± 1.5%, as confirmed by trypan blue staining (**Supplementary Fig. 8**). This high viability may be due to the fact that the cells were sorted based on TMRM accumulation (and thus contained active mitochondria). We cultured the sorted cells for 7 d to allow the cells to attach to the substrate and to elongate (Online Methods). Immunofluorescence staining for α-actinin and Nkx2.5 in three independent experiments confirmed that these cells were high-purity cardiomyocytes (99.5 ± 0.3%; **Fig. 3e**). We obtained >99% pure ESC-derived cardiomyocytes from day 12–25 embryoid bodies (**Fig. 3f**). We also obtained highly pure cardiomyocytes from mouse iPSCs (**Fig. 3g,h**).

To investigate the possibility of isolating cardiac progenitor cells, we stained whole E7.5 and E7.75 embryos. We found that TMRM faintly, but distinctly, marked the cardiac crescent, which contains cardiomyogenic precursor cells, indicating a possible applicability of our method to obtaining progenitor cells. Next, we carried out time-lapse fluorescence microscopy on attached mouse embryoid bodies stained with TMRM (**Supplementary Fig. 9**). We first observed TMRM-positive cells on day 6.5. Fluorescence in these cells increased gradually between days 6.5 and 7 and they started beating on day 7.0. In contrast, TMRM-negative cells did not beat during the experiments. We then performed FACS analysis on dissociated cells obtained from day 3–6.5 embryoid bodies and stained with TMRM. There were no cells in fraction 1. The higher TMRM-fluorescence cells in fraction 2 from day 3 and 4 embryoid bodies did not differentiate into cardiomyocytes, even after subsequent culture of attached cells for up to 8 d. In the case of day 6.5 embryoid bodies, some of the isolated cells differentiated into cardiomyocytes upon subsequent culture for 3 d. We also stained *Nkx2.5-GFP* knock-in mouse ESCs[6], which we and others have used frequently to isolate cardiomyocytes. After embryoid body formation, we first observed GFP fluorescence on day 7, whereas we observed TMRM staining on day 6.5 (**Supplementary Fig. 10**). Our observations indicate that our method can be used to purify differentiated cardiomyocytes but not cardiac progenitor cells.

We differentiated common marmoset ESCs, human ESCs and human iPSCs into cardiomyocyte-containing embryoid bodies by conventional floating cell culture. We transferred the embryoid bodies into the cell-attachment dishes with 10 nM TMRM. Beating embryoid bodies had extremely high TMRM fluorescence compared with that of nonbeating embryoid bodies derived from marmoset and human ESCs (**Fig. 4a**). Then we dispersed embryoid body–derived cells, stained them with TMRM and analyzed them on a FACS (**Fig. 4b**). We fixed sorted human

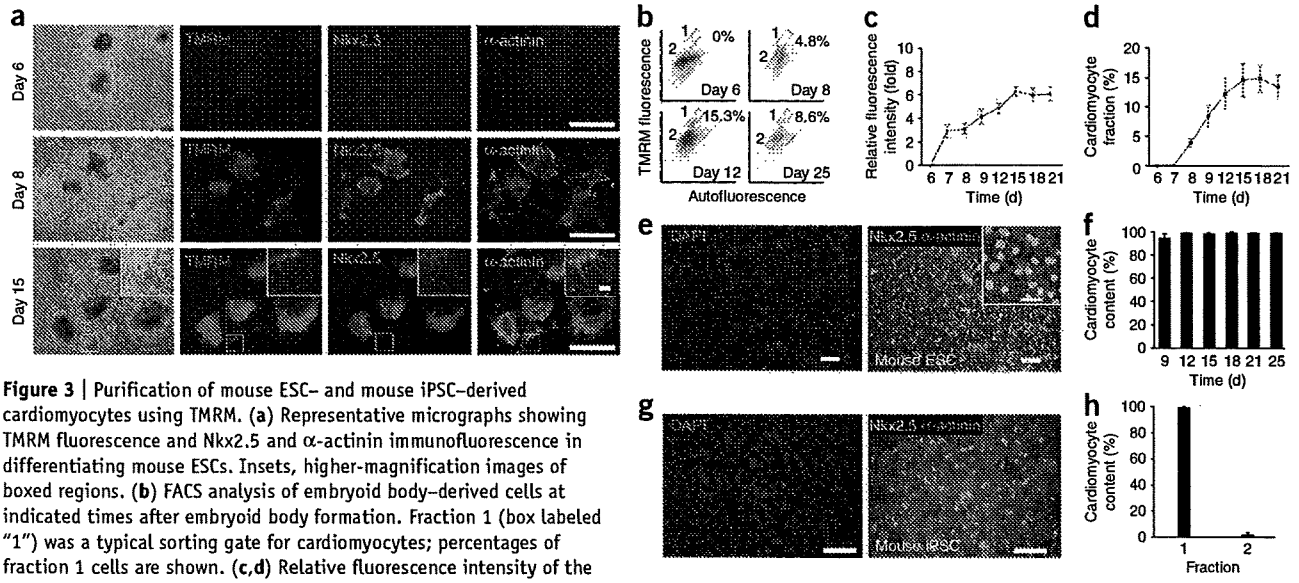

Figure 3 | Purification of mouse ESC- and mouse iPSC-derived cardiomyocytes using TMRM. (**a**) Representative micrographs showing TMRM fluorescence and Nkx2.5 and α-actinin immunofluorescence in differentiating mouse ESCs. Insets, higher-magnification images of boxed regions. (**b**) FACS analysis of embryoid body–derived cells at indicated times after embryoid body formation. Fraction 1 (box labeled "1") was a typical sorting gate for cardiomyocytes; percentages of fraction 1 cells are shown. (**c**,**d**) Relative fluorescence intensity of the fraction 1 versus fraction 2 cells (**c**) and percentage of cells in fraction 1 (**d**) over time. Data are mean ± s.d. ($n = 3$). (**e**–**h**) Immunofluorescence staining for Nkx2.5 and α-actinin in cultured fraction 1 cells sorted from day 15 embryoid bodies differentiated from mouse ESCs (**e**) and from mouse iPSCs (**g**); and cardiomyocyte content in cultured cells sorted from day 9–25 embryoid bodies differentiated from mouse ESCs (**f**) and in cultured cells sorted from day 15 embryoid bodies differentiated from mouse iPSCs (**h**). Data are mean ± s.d. ($n = 3$). Scale bars, 1 mm (**a**); and 100 μm (**a** inset, **e**,**g**).

cells in fraction 1, immunostained them for Nkx2.5 and subjected them to a second FACS analysis. The results showed that over 99.9% of cells in fraction 1 were cardiomyocytes (**Fig. 4c**). Furthermore, we compared expression of cardiac and noncardiac genes in human ESC–derived cardiomyocytes isolated by our method and in unpurified cells from embryoid bodies using real-time PCR. We observed a marked increase in the expression of myocardial genes and a decrease in the expression of nonmyocardial genes in purified human ESC–derived cardiomyocytes (**Supplementary Fig. 11**).

We also cultured the sorted cells for 5 d and immunostained them for Nkx2.5 and α-actinin (**Fig. 4d**). Common marmoset ESC, human ESC and human iPSC fraction 1 comprised 99.0 ± 1.0%, 99.0 ± 0.9% and 99.3 ± 0.2% cardiomyocytes, respectively; in contrast, fraction 2 had 2.3 ± 0.6%, 2.5 ± 0.2% and 1.7 ± 1.6% cardiomyocytes, respectively (**Fig. 4e**). To estimate the acquisition efficiency in the sorting experiments, we compared by FACS analysis the cardiomyocyte fraction obtained by TMRM with that obtained by immunofluorescence staining for α-actinin. The number of cardiomyocytes isolated by TMRM staining was 60–90% of the number defined by α-actinin staining (**Supplementary Fig. 12**). To rule out the possibility of skeletal muscle contamination in the sorted cardiomyocyte population, we extracted total mRNA from sorted cardiomyocytes and evaluated it for *myoD* expression using real-time PCR. We confirmed that there was no amplification of *myoD* (**Supplementary Fig. 13**).

No teratoma formation

We cultured the purified mouse ESC-derived cardiomyocytes and noncardiomyocytes for 7 d and found that although noncardiomyocytes formed piled-up colonies, in which some cells

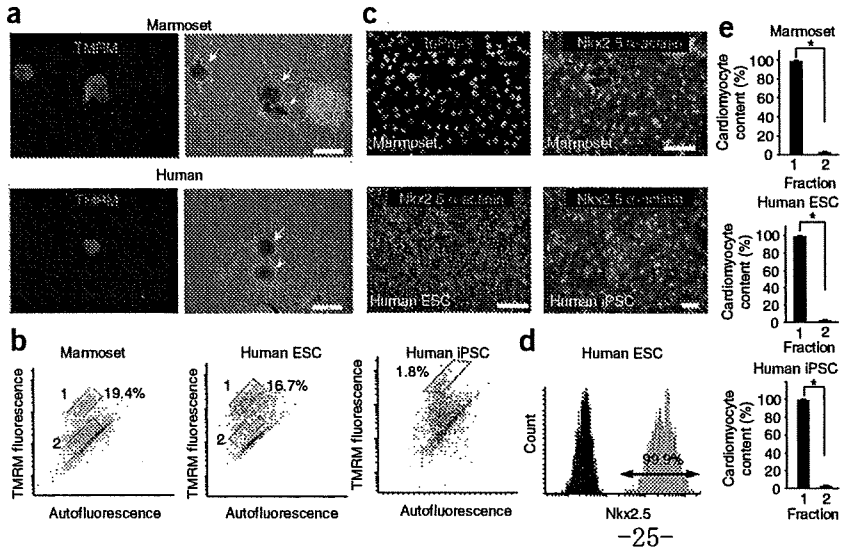

Figure 4 | Purification of PSC-derived cardiomyocytes in human and marmoset. (**a**) TMRM fluorescence (left) and phase contrast (right) images of marmoset and human embryoid bodies containing beating cardiomyocytes. Arrows, beating areas; arrowheads, nonbeating areas. (**b**) FACS separation of TMRM-stained cardiomyocytes derived from common marmoset ESCs, human ESCs and human iPSCs. Fractions 1 and 2 are boxed; percentages of fraction 1 cells are shown. (**c**) Immunofluorescence staining of fraction 1 cells for α-actinin and Nkx2.5. ToPro-3 represents nuclear staining. (**d**) Histogram showing immunodetection of Nkx2.5 (gray) and negative control (without first antibody; black) in sorted human ESC–derived fraction 1 cells. (**e**) The cardiomyocyte content of fractions 1 and 2 in common marmoset ESCs, human ESCs and human iPSCs. Data are mean ± s.d. ($n = 3$). *$P < 0.01$ (Student *t*-test). Scale bars, 500 μm (**a**); and 100 μm (**c**).

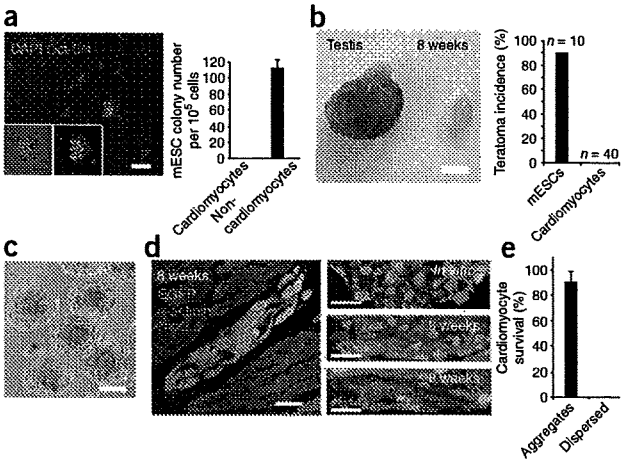

Figure 5 | Transplantation of purified mouse ESC-derived cardiomyocytes. (**a**) Immunofluorescence staining for Oct3/4 (red) in the sorted cells from the noncardiac fraction (left), and numbers of mouse ESC-like colonies obtained from 10^5 sorted cells (right). Data are mean ± s.d. (n = 3). (**b**) Transplantation of 250 undifferentiated mouse ESCs into testes resulted in teratoma formation (testis), whereas transplantation of 1.9×10^5 purified mouse ESC-derived cardiomyocytes did not (8 weeks). Incidence of teratoma formation was quantified (right). (**c**) Phase contrast image of mouse cardiomyocyte aggregates. (**d**) Immunofluorescence staining of engrafted mouse cardiomyocyte aggregates for α-actinin and Nkx2.5 8 weeks after transplantation (left); transplanted cells expressed EGFP. Mouse ESC-derived cardiomyocytes *in vitro* and 3 and 8 weeks after transplantation immunostained for Nkx2.5 and α-actinin (right). (**e**) Transplanted mouse ESC-derived cardiomyocyte survival. Data are shown as mean ± s.d. (n = 5). Scale bars, 100 μm (**a**,**c**); 5 mm (**b**); and 20 μm (**d**).

were positive for Oct3/4, the cardiomyocytes did not (**Fig. 5a**). Further, we transplanted 1.9×10^5 aggregated mouse ESC–derived cardiomyocytes and 250 undifferentiated mouse ESCs as a control into the testes of immunocompromised nonobese diabetic–severe combined immunodeficient (NOD-SCID) mice. Two months later, 90% of the control mice developed teratomas (9 of 10 mice), but we did not detect teratomas in any of the mice transplanted with purified mouse ESC–derived cardiomyocytes (0 of 40 mice) (**Fig. 5b**). We tried to verify that there was no teratoma formation in the heart by directly injecting mouse ESC–derived cardiomyocytes (1×10^5) into the myocardium of five NOD-SCID mice immediately after sorting. Two months later, we found few (<1%) of the transplanted cardiomyocytes in the heart (data not shown).

To understand the mechanism underlying this cell loss, we injected purified and MitoTracker Red–labeled neonatal rat cardiomyocytes into the left ventricular free wall of *ex vivo*–perfused hearts. We found one-third to one-half of injected cells in the postperfusion solution, indicating that the neonatal rat cardiomyocytes were washed out within the first 10 min (**Supplementary Fig. 14**). Next, we compared the tissue adhesiveness of purified mouse ESC–derived cardiomyocytes and mouse embryonic fibroblasts (MEFs) by counting cells in continuous sections of whole ventricles 24 h after injection into the left ventricular free walls. We found that less than 1% of the grafted ESC-derived cardiomyocytes had adhered to the host myocardium, compared with 50% of MEFs.

Transplantation of PSC-derived cardiomyocytes

From the above observations, we reasoned that loss of transplanted ESC-derived cardiomyocytes may be due to rapid washout and low adhesiveness of the cells. Because ESC-derived cardiomyocytes existed as homophilic cell aggregates (diameter, 100–500 μm) in mouse, marmoset and human embryoid bodies (**Supplementary Fig. 15**), we suspected that re-aggregated purified ESC-derived cardiomyocytes may be more resistant to rapid washout. We generated cardiomyocyte aggregates by seeding 313–10,000 purified mouse ESC–derived cardiomyocytes onto nonadhesive 96-well plates. One day after seeding, the cells adhered to each other, aggregated and started synchronized beating; 5 d later, cardiomyocyte aggregates formed with diameters of 100–450 μm (**Fig. 5c**, **Supplementary Fig. 16** and **Supplementary Video 2**). Propidium iodide staining revealed that a high proportion of re-aggregated mouse ESC–derived cardiomyocytes were viable (98.8 ± 0.2% of seeded cells; **Supplementary Fig. 16**).

We transplanted mouse cardiomyocyte aggregates into the ventricular free walls of NOD-SCID mice and killed the mice at 3 and 8 weeks (n = 5 for both groups). We observed no teratoma formation in either group. Immunofluorescence staining revealed that cell aggregates positive for the tracers Nkx2.5 and α-actinin were located in the left ventricle (**Fig. 5d**). The number of cells that survived in the heart was greater than 90% (**Fig. 5e**). Furthermore, we repeated these experimental procedures using purified human ESC–derived cardiomyocytes (**Supplementary Video 3**). Two months after transplantation, we detected a large amount of human myocardial tissue in NOD-SCID mouse heart (**Supplementary Fig. 17**).

Finally, we investigated which autoparacrine factors are important for the survival of ESC-derived cardiomyocytes. Human cardiomyocyte aggregates remained viable under serum-free culture conditions; moreover, their diameters increased by approximately twofold by day 25. Supplementation of the cultures with physiological concentrations of basic fibroblast growth factor (bFGF), epidermal growth factor (EGF), platelet-derived growth factor beta dimer (PDGF-BB) and endothelin-1 (ET-1) strongly enhanced the growth of the cardiomyocyte aggregates (**Supplementary Fig. 18a** and **Supplementary Video 4**). We confirmed expression of these growth factors and their receptors by real-time PCR (probe and primer sets are listed in **Supplementary Table 1**). We also confirmed that these growth factors were expressed in adult human and mouse hearts (**Supplementary Fig. 18b**). Autoparacrine stimulation with these growth factors may be one reason why grafted cardiomyocyte aggregates survived and grew in the host myocardium.

DISCUSSION

Our method for cardiomyocyte isolation has two advantages. First, it does not require genetic modification of the cells. Genetic modifications using nonviral or viral systems have several disadvantages: extrinsic genes may be silenced, the number of integration events in one cell is difficult to control, targeted integration is not straightforward, and line selection as well as verification of proper expression of extrinsic genes[14] is time-consuming. Furthermore, genetic modification carries risks such as possible tumor formation[15–17]. Second, our method is likely to be widely applicable. We demonstrated that it may be used to purify ESC-derived cardiomyocytes in four species, including human,

and that it is also applicable to mouse and human iPSCs. High abundance of cellular mitochondria is likely to be a common characteristic of cardiomyocytes irrespective of species. In contrast, most genetic modifications require species-specific constructs. Our simple purification strategy should facilitate basic studies using embryonic heart and stem cell–derived cardiomyocytes; furthermore, this strategy can also allow isolation of noncardiomyocytes, which may open up new approaches to studying developmental interactions.

The ESC-derived cardiomyocytes purified using our method did not induce teratoma formation in either the heart or testes. Although from the viewpoint of clinical safety, further studies using large animal models with a much larger number of ESC-derived cardiomyocytes will be required, we believe that our purification method may have considerable advantages over existing methods for eventual clinical translation as well.

Our results suggest that induction of mitochondrial biogenesis begins shortly before beating of cardiomyocytes. This indicates the tight relationship between cardiomyogenesis and mitochondrial biogenesis. A combination of our strategy and other marking techniques for cardiac progenitor cells may facilitate study in this field.

Unpurified fetal and neonatal rat cardiomyocytes and bone marrow mesenchymal and ESC-derived cardiomyocytes have been shown to survive in the recipient heart[18–20]. In contrast, purified and dispersed cardiomyocytes differentiated from ESCs did not achieve a high survival rate[5]. Re-aggregation augmented the long-term survival of purified mouse and human ESC–derived cardiomyocytes. Our results indicate that ESC-derived cardiomyocytes might be highly anchorage-dependent, and that homophilic cell-to-cell adhesion and autoparacrine signaling may be important factors contributing to their survival.

METHODS

Methods and any associated references are available in the online version of the paper at http://www.nature.com/naturemethods/.

Note: Supplementary information is available on the Nature Methods website.

ACKNOWLEDGMENTS

Human ESCs were a gift of N. Nakatsuji at the Department of Development and Differentiation, Institute for Frontier Medical Sciences, Kyoto University. Human and mouse iPSCs were a gift of S. Yamanaka at the Center for iPS Cell Research and Application, Institute for Integrated Cell-Material Sciences, Kyoto University. Mouse ESCs were a gift of H. Niwa at the Laboratory of Pluripotent Cell Studies, RIKEN Center for Developmental Biology. This study was supported in part by research grants from the Ministry of Education, Science and Culture, Japan, and by the Program for Promotion of Fundamental Studies in Health Science of the National Institute of Biomedical Innovation.

AUTHOR CONTRIBUTIONS

F.H. designed the whole study. F.H. performed most experiments and wrote the manuscript. H.C. participated in cell-sorting experiments and prepared cells. H.Yamashita participated in cell-sorting experiments, PCR experiments, immunofluorescent staining, animal experiments and preparing cells. S.T., Y.S., W.L., T.T., T.O., K.S., Y.O. and T.E. participated in cell preparations. H.Yamakawa and M.M. participated in heart perfusion experiments. K.H. and T.M. provided the *Nkx2.5 knock-in* ESCs. S.Y., M.M., R.K., M.S., S.M. and S.O. provided advice. E.S. provided cmESCs. T.S. supervised Y.S. K.F. provided advice, obtained the budget and supervised the project.

COMPETING INTERESTS STATEMENT

The authors declare competing financial interests: details accompany the full-text HTML version of the paper at http://www.nature.com/naturemethods/.

Published online at http://www.nature.com/naturemethods/.
Reprints and permissions information is available online at http://npg.nature.com/reprintsandpermissions/.

1. Yuasa, S. *et al.* Transient inhibition of BMP signaling by Noggin induces cardiomyocyte differentiation of mouse embryonic stem cells. *Nat. Biotechnol.* **23**, 607–611 (2005).
2. Nemir, M., Croquelois, A., Pedrazzini, T. & Radtke, F. Induction of cardiogenesis in embryonic stem cells via downregulation of Notch1 signaling. *Circ. Res.* **98**, 1471–1478 (2006).
3. Mummery, C. *et al.* Differentiation of human embryonic stem cells to cardiomyocytes: role of coculture with visceral endoderm-like cells. *Circulation* **107**, 2733–2740 (2003).
4. Anderson, D. *et al.* Transgenic enrichment of cardiomyocytes from human embryonic stem cells. *Mol. Ther.* **15**, 2027–2036 (2007).
5. Kolossov, E. *et al.* Engraftment of engineered ES cell-derived cardiomyocytes but not BM cells restores contractile function to the infarcted myocardium. *J. Exp. Med.* **203**, 2315–2327 (2006).
6. Hidaka, K. *et al.* Chamber-specific differentiation of Nkx2.5-positive cardiac precursor cells from murine embryonic stem cells. *FASEB J.* **17**, 740–742 (2003).
7. Fijnvandraat, A.C. *et al.* Cardiomyocytes purified from differentiated embryonic stem cells exhibit characteristics of early chamber myocardium. *J. Mol. Cell. Cardiol.* **35**, 1461–1472 (2003).
8. Gassanov, N., Er, F., Zagidullin, N. & Hoppe, U.C. Endothelin induces differentiation of ANP-EGFP expressing embryonic stem cells towards a pacemaker phenotype. *FASEB J.* **18**, 1710–1712 (2004).
9. Huber, I. *et al.* Identification and selection of cardiomyocytes during human embryonic stem cell differentiation. *FASEB J.* **21**, 2551–2563 (2007).
10. Klug, M.G., Soonpaa, M.H., Koh, G.Y. & Field, L.J. Genetically selected cardiomyocytes from differentiating embronic stem cells form stable intracardiac grafts. *J. Clin. Invest.* **98**, 216–224 (1996).
11. Laflamme, M.A. *et al.* Cardiomyocytes derived from human embryonic stem cells in pro-survival factors enhance function of infarcted rat hearts. *Nat. Biotechnol.* **25**, 1015–1024 (2007).
12. Xu, C., Police, S., Hassanipour, M. & Gold, J.D. Cardiac bodies: a novel culture method for enrichment of cardiomyocytes derived from human embryonic stem cells. *Stem Cells Dev.* **15**, 631–639 (2006).
13. Monici, M. Cell and tissue autofluorescence research and diagnostic applications. *Biotechnol. Annu. Rev.* **11**, 227–256 (2005).
14. Gropp, M. & Reubinoff, B. Lentiviral vector-mediated gene delivery into human embryonic stem cells. *Methods Enzymol.* **420**, 64–81 (2006).
15. Tsukahara, T. *et al.* Murine leukemia virus vector integration favors promoter regions and regional hot spots in a human T-cell line. *Biochem. Biophys. Res. Commun.* **345**, 1099–1107 (2006).
16. Recchia, A. *et al.* Retroviral vector integration deregulates gene expression but has no consequence on the biology and function of transplanted T cells. *Proc. Natl. Acad. Sci. USA* **103**, 1457–1462 (2006).
17. Woods, N.B. *et al.* Lentiviral vector transduction of NOD/SCID repopulating cells results in multiple vector integrations per transduced cell: risk of insertional mutagenesis. *Blood* **101**, 1284–1289 (2003).
18. van Laake, L.W. *et al.* Human embryonic stem cell-derived cardiomyocytes survive and mature in the mouse heart and transiently improve function after myocardial infarction. *Stem Cell Rev.* **1**, 9–24 (2007).
19. Reinecke, H., Zhang, M., Bartosek, T. & Murry, C.E. Survival, integration, and differentiation of cardiomyocyte grafts: a study in normal and injured rat hearts. *Circulation* **100**, 193–202 (1999).
20. Hattan, N. *et al.* Purified cardiomyocytes from bone marrow mesenchymal stem cells produce stable intracardiac grafts in mice. *Cardiovasc. Res.* **65**, 334–344 (2005).

T-box 2, a mediator of Bmp-Smad signaling, induced hyaluronan synthase 2 and Tgfβ2 expression and endocardial cushion formation

Manabu Shirai[a], Kyoko Imanaka-Yoshida[b], Michael D. Schneider[c], Robert J. Schwartz[d,1], and Takayuki Morisaki[e]

[a]Department of Bioscience, National Cardiovascular Center Research Institute, 5-7-1 Fujishirodai, Suita, Osaka 565-8565, Japan; [b]Department of Pathology and Matrix Biology, Mie University Graduate School of Medicine, 2-174 Edobashi, Tsu, Mie 514-8507, Japan; [c]Faculty of Medicine, National Heart and Lung Institute Imperial College London, London SW7 2AZ United Kingdom; [d]Institute of Biosciences and Technology, Texas A&M University System Health Science Center, 2121 West Holcombe Boulevard, Houston, TX 77030; and [e]Department of Molecular Pathophysiology, Osaka University Graduate School of Pharmaceutical Sciences, 1-6 Yamadaoka, Suita, Osaka 565-0871, Japan

Edited by Eric N. Olson, The University of Texas Southwestern Medical Center, Dallas, TX, and approved September 11, 2009 (received for review January 21, 2009)

During early heart development, Tbx2 gene expression is initiated in the cardiac crescent and then becomes restricted to the outflow tract and the atrioventricular region. We identified a *Tbx2* regulatory region, enriched in multiple Smad sites, sufficient to reproduce *Tbx2* expression patterns overlapping Bmp2 and Bmp4 gene activity in the heart. The role of *Tbx2* in cardiogenesis was analyzed by using Cre-LoxP activated *Tbx2* transgenic misexpression in chamber myocardium. Ventricular *Tbx2* misexpression exhibited an abnormally narrow chamber lumen owing to the expansion of *Hyaluronan synthase 2* expression in the ECM or cardiac jelly and the appearance of the endocardial cushions (ECs). Excessive *Tbx2* also induced *Tgfβ2*, which coincided with the outgrowth epithelial-mesenchymal transformed cells in ventricular and atrial tissues modifying cardiomyocyte identity from chamber type to non-chamber type. *Tbx2*, a central intermediary of Bmp-Smad signaling, has a central part in directing *Has2* and *Tgfβ2* expression, facilitating EC formation.

cardiac jelly | cardiomyocyte identity | epithelial-mesenchymal transformation | extracellular matrix | misexpression

The heart develops, as a modular organ, driven by distinct transcriptional regulatory programs that control each anatomical region (1). A member of the T-box factor family, *Tbx2*, which first appears in the cardiac crescent and then later restricted to non-chamber myocardium (My) [outflow tract (OFT), atrioventricular canal (AVC), inner curvature, and inflow tract) (2, 3)], is a valuable model of modular cardiac gene activity. *Tbx2* is central for endocardial cushion (EC) formation and chamber specification, and may be a transcriptional repressor (4, 5). Expression of chamber-specific myocardial genes, which include *Nppa* (encoding atrial natriuretic factor, *ANF*), *Gja5* (encoding connexin 40, *Cx40*), and *Gja1* (encoding connexin 43, *Cx43*), were repressed by *Tbx2* (3–5). *Tbx2* null mutant embryos exhibited small AVC and defective OFT septation (3), whereas *Tbx2* transgenic expression blocked chamber formation (4) and cell proliferation in the OFT and AVC (6).

The ECs form from localized expansion of the ECM also named cardiac jelly (7, 8) found in the cardiac OFT and AVC segments the simple heart tube into a complicated structure composed of the aortic sac, common ventricular chamber, and atrial chamber. Some endocardial cells invade into the ECM through epithelial-mesenchymal transformation (EMT) to remodel the cushion tissue into the mature valves. Several signaling pathways have been implicated in EC formation. The Bmp pathway is essential for both processes; expansion of ECM and EMT in the EC formation (9–14). Tgfβ2 performs crucial and sequential roles in EC formation and may also be regulated by Bmp2/4 during cardiogenesis (9–11). The hyaluronan (HA) synthase 2 (*Has2*) has been recently shown to have essential role in expansion of ECM and EMT (16). Also, *Tbx2* may be a direct target of Bmp2/4 signaling pathway during EC formation (2).

Here, we delineated an 80-bp regulatory region within the *Tbx2* 5′ flanking sequences, which contain multiple Smad DNA binding sites that recapitulate expression of *Tbx2* in the AVC and OFT. Previously, myocardial-specific inactivation of *Bmp2* also inhibited the appearance of several factors, including *Tbx2*, *Tgfβ2*, and *Has2*, and blocked cushion formation (9). To define the regulatory hierarchy shared by Bmp2/4-dependent genes, we analyzed embryos in which murine *Tbx2* was misexpressed in the developing chamber My, using a mouse genetic system based on Cre/loxP recombination. *Tbx2* altered cardiogenic lineage specification by expanding the ECM and EMT to drive EC formation via the induction of Tgfβ2 and Has2 gene activity in embryonic hearts.

Results

Smad Signaling Drives *Tbx2* Transgene Activity via a Distal Enhancer. *Tbx2* expression was first detected in the cardiac crescent and notochordal plate (Fig. 1*A*). At E8.5, *Tbx2* expression was maintained only in the posterior portion of the looping heart (Fig. 1*B*). As the heart matured, the expression of *Tbx2* became further limited to the AVC and OFT region (Fig. 1 *E* and *F*). *Tbx2* mRNA was also detected in the optic cups, otic vesicles, pharyngeal arches, and limb buds of embryonic day (E)9.5 and E10.5 mouse embryos (Fig. 1 *C* and *D*). Transient F_0 transgenic mice harboring 4.1 kilobase (kb) of Tbx2 5′ flanking sequences linked to the *lacZ* reporter gene (Fig. 1*K*) revealed β-galactosidase activity in the OFT, AVC, and a portion of the left atrium, whereas LacZ activity was absent from the right atrium and the ventricles (Fig. 1*L*). Also, *Tbx2*, a downstream target of murine Bmp2/4 signaling (2, 9), was colocalized to the AVC and OFT (Fig. 1 *G–J*). After serial and gap deletion mutagenesis strategy, recapitulated *Tbx2* expression was delineated to a region between −3.4 and −2.6 kb in transgenic mouse embryos (Fig. 1 *L–O*).

Paired Smad 1/4 proteins, primary intracellular mediators of Bmp signals (12), activated transcription of the −4.1-kb reporter construct (Fig. 2*A*). Other Smad factor combinations did not strongly activate the *Tbx2* reporter, whereas the inhibitory Smad 6 (13, 14) blocked Tbx2 gene activity. *Tbx2* regulatory region

Author contributions: M.S., K.I.-Y., M.D.S., R.J.S., and T.M. designed research; M.S. performed research; M.D.S. contributed new reagents/analytic tools; M.S., K.I.-Y., R.J.S., and T.M. analyzed data; and M.S., K.I.-Y., R.J.S., and T.M. wrote the paper.

The authors declare no conflict of interest.

This article is a PNAS Direct Submission.

[1]To whom correspondence should be addressed. E-mail: rschwartz@ibt.tamhsc.edu.

This article contains supporting information online at www.pnas.org/cgi/content/full/0900635106/DCSupplemental.

www.pnas.org/cgi/doi/10.1073/pnas.0900635106

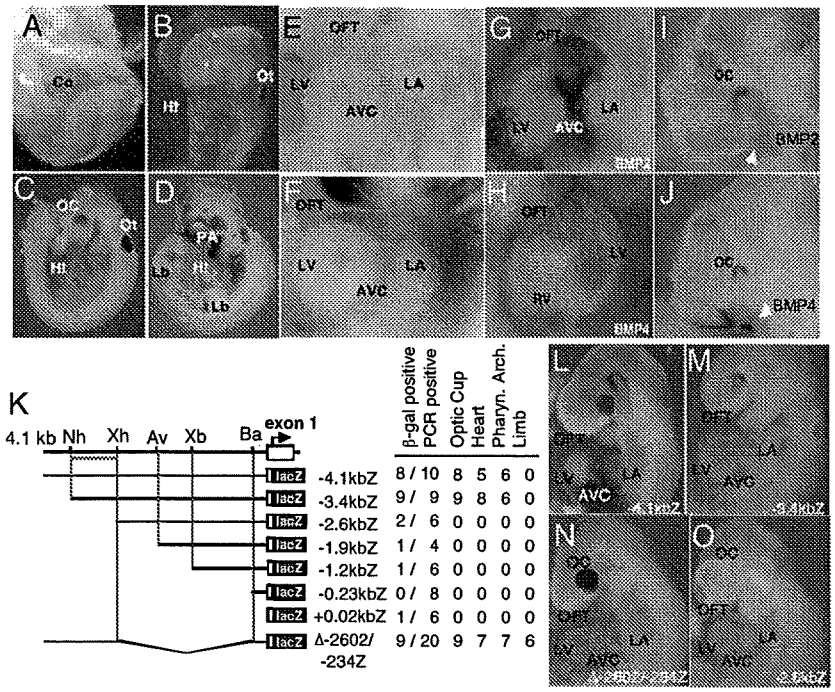

Fig. 1. Mouse Tbx2 gene activity in early cardiac development was recapitulated by distal *cis*-acting regulatory regions coincided with *Bmp2* and *Bmp4* expression. *Tbx2* expression was first detected in the cardiac crescent at E7.5 (*A*), and restricted to the posterior part of looping heart at E8.5 (*B*). The expression of *Tbx2* was also observed in the developing eye, otic cup, pharyngeal arches, and limb buds (*B*–*D*) At E9.5 and E10.5, *Tbx2* transcripts were localized in the OFT and AVC (*E* and *F*).. Expression of *Bmp2* and *Bmp4* (*G* and *H*) was observed in the OFT and AVC (*I* and *J*). Schematic representation of serial deleted 5′ flanking sequences of the Tbx2 gene, which were analyzed for transgene expression patterns in E9.5–E10.5 F_0 founder embryos (*K*). An upstream regulatory region that directs Tbx2 gene expression was indicated by a red bar. *LacZ* was expressed in the optic cup, heart, and pharyngeal arches using 4.1 kb (*L*), 3.4 kb (*M*), and Δ−2602/−234 (*N*) 5′ flanking fragments. No LacZ staining was observed in −2.6-kbZ transgenic embryos (*O*). Cc, cardiac crescent; Ht, heart; LA, left atrium; Lb, limb bud; LV, left ventricle; OC, optic cup; Ot, otic cup; PA, pharyngeal arch. Restriction sites shown above are: Nh, NheI; Xh, XhoI; Av, AvrII; Xb, XbaI; and Ba, BamHI.

responsive to Bmp signaling was localized to a 290-bp region expression in the developing heart (Fig. 2 *B* and *C*), which contains at least five conserved Smad sites, two of which, SBE1 and SBE5 sequences, were potent Smad1/4 cofactor binding sites (Fig. S1). Schematic representation of *Tbx2* transgenes analyzed in E9.5 F_0 embryos and a summary of the tissue restricted expression activity is shown in Fig. 2*C*, whereas five SMAD sites in SBE1-5 were mutated by site directed mutagenesis as shown in mSBE1-5 (Fig. 2*D*). The gap deletion mutant Δ−2899/−2602 hsp68lacZ construction, in which the five Smad sites were removed from the *Tbx2* 5′ flanking sequence, showed a complete loss of *lacZ* expression activity in the hearts of F_0 transgenic embryos (Fig. 2 *C* and *F*). The Smad site enriched region (SBE; −2916/−2602) linked to a minimal *hsp68* promoter *lacZ* transgene, revealed robust expression in the OFT and AVC, sufficient to recapitulate the restricted *Tbx2* expression pattern in the heart (Fig. 2 *C* and *G*), whereas site directed Smad site mutations eliminated gene activity in transgenic mice (Fig. 2 *C* and *H*).

Abnormal Deposition of ECM in *mTbx2*-Misexpressing Embryonic Hearts. To study the role of *Tbx2* in the cardiac morphogenesis, we generated transgenic mice that conditionally misexpressed murine Tbx2 gene in embryonic chamber-cardiomyocytes (Fig. 3 *A* and *B*; Fig. S2). Activated *Tbx2* embryos exhibited enlarged hearts, with marked myocardial hypoplasia associated with rich deposition of ECM in the compact and trabecular My (Fig. 3 *C* and *D*). Expansion of the EC (cardiac jelly) between the endocardium (En) and My (Fig. 3*E*) stained with alcian blue for acidic glycosaminoglycans (15) caused a narrow ventricular lumen. In control littermates, acidic glycosaminoglycans were deposited mainly in the ECM of OFT and AVC regions at E10.5 compared with the expanded ECM induced by activated *Tbx2*.

Glycosaminoglycan HA, a major constituent of the cardiac jelly, may be required for the expansion of EC (16,17). Excessive acidic glycosaminoglycans deposited through the cardiac tube in *mTbx2*-misexpressing embryos were also revealed by deposition of HA with the biotinylated-HA binding protein (BP; Fig. 3*F*). The specific binding of HABP to HA was eliminated by hyaluronidase treatment (Fig. S3). HA deposition was observed between the En and My in the inner curvature and the AVC of both control littermates and *mTbx2*-misexpressed mice, and in between the En and My of the outer curvature of *mTbx2*-misexpressed ventricles (Fig. 3*F*). Also, cultured cardiomyocytes from quartered hearts identified by *lacZ* and or by *Myh6* induced *mTbx2* expression (Fig. 3*G*; Fig. S4) were classified by the amount of HA secretion (Fig. 3*H*). *Tbx2*-misexpressing ventricular myocytes secreted greater amount of HA compared with ventricular myocytes from control littermates.

***Has2* and *Tgfβ2* are *Tbx2* Downstream Gene Targets.** Is there a hierarchical relationship between *Tbx2*, *Has2*, and *Tgfβ2*? HA synthatase (Has)2, the major enzyme responsible for HA synthesis in the AVC and atria, was strongly up-regulated in the ventricular My by *mTbx2* misexpression (Fig. 4). In comparison, other components of the ECM, including *Col1a1* (encoding type I collagen), *Cspg2* (encoding chondroitin sulfate proteoglycan 2, *versican*), *Fn1* (encoding fibronectin 1), and *Tnc* (encoding tenascin C) did not show obvious differences (data not shown). *Has2* is a direct Tbx2 target, because T-box binding sites were conserved between *Has2* promoter regions, which recruited en-

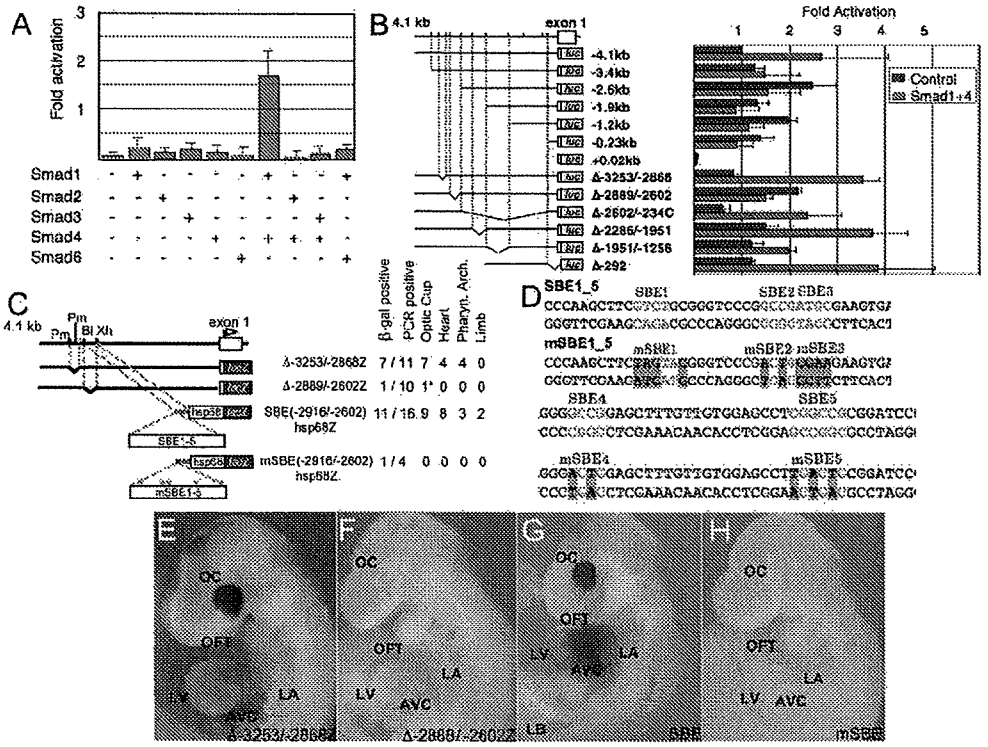

Fig. 2. Delineation of the distal Smad factor dependent *Tbx2* enhancer. (*A*) Multiple Smad expression vectors tranfected into CV1 cells revealed activation caused by Smad1/4 of the 4.1 kb of 5′ flanking sequence of *Tbx2* fused in-frame to the luciferase. The bars represent the average of three independent transfections, and the error bars represent the SE of corrected luciferase activity relative to the pCMV5 control vector. (*B*) Activation by Smad1/4 required the −2889/−2602 region. (*C*) Schematic representation of *Tbx2* transgenes analyzed in E9.5 F_0 embryos and a summary of the tissue restricted expression activity. (*D*) Five SMAD sites in SBE1-5 were mutated by site directed mutagenesis in mSBE1-5. (*E–J*) *LacZ* expression patterns in E9.5 F_0 embryos. (*E*) Δ−3253/−28682hsp68Z transgene; a gap deletion mutant, of a region immediately upstream of the multiSmad sites. (*F*) Δ−2899/−2602hsp68lacZ; a gap deletion mutant in which the multiple Smad sites were removed from the 5′ flanking sequence. (*G*) SBE(−2916/−2602)hsp68lacZ; the region from −2916 to −2602bp, containing five Smad sites, was linked to the hsp68lacZ reporter gene. (*H*) mSBE(−2916/−2602)hsp68lacZ; mutations were inserted at the multiple Smad sites in the −2916/−2602 fragment. *LacZ* expression were recapitulated by the DNA fragments containing Smad binding sites (*E* and *G*), whereas gap deletion and point mutagenesis of Smad binding sites eliminated gene activity in transgenic mice (*F* and *H*). Restriction sites are: *Bl*pI; Xh, XhoI.

dogenous Tbx2 from cardiac nuclear chromatin extracts and was transactivated by *Tbx2* (*SI Materials and Methods* and Fig. S5).

Tgfβ2 is normally expressed in the myocardial cells in the OFT and AVC, but was induced by *Myh6-Cre* activated *mTbx2* in ventricular and atrial My (Fig. 5 *A* and *B*). Also, phosphorylated Smad2 appeared in the endocardial and myocardial cells of *mTbx2*-activated ventricles and atria (Fig. 5*C*), which coincided with robust in vitro EMT assays (Fig. 5 *D* and *E*); thus, suggesting that the Tgfβ2 signaling pathway was activated by *mTbx2*. *Tgfβ2* may also be a direct target of Tbx2, because the *Tgfβ2* promoter has conserved T-box binding sites, bound endogenous Tbx2, and was activated with a *Tbx2*-expression vector (*SI Materials and Methods* and Fig. S6).

Discussion

Smad Factor Signaling Directed *Tbx2* Expression Through a Distal Enhancer During Early Murine Cardiogenesis. *Tbx2* transcripts first appear in the cardiac crescent and then later became restricted to the OFT and AVC during early avian (2) and mouse embryogenesis (Fig. 1). *Tbx2* is also expressed in the embryonic limb, optic cup, otic cup, and pharyngeal arches. Approximately 4 kb of 5′ flanking sequence of the murine Tbx2 gene was sufficient to reproduce much of these mouse embryonic expression patterns, as a *lacZ* reporter transgene. *LacZ* expression patterns closely overlapped with those of *Bmp2* and *Bmp4* in the heart and eye, and was delineated within the *Tbx2* 5′ flanking sequences, which contained Bmp directed multiple high-affinity binding sites for Smad transcription factors. Removal of these multiple Smad sites by gap deletion mutagenesis from the 4-kb flanking sequences blocked reporter gene activity in early embryos. In contrast, this short enhancer region linked to a minimal *hsp68* promoter was sufficient for steering the restricted expression of *lacZ* in a pattern, highly similar to the endogenous Tbx2 gene activity. Previously, application of Bmp2 selectively induced *cTbx2* expression in noncardiogenic embryonic tissue, and the Bmp antagonist Noggin down-regulated *cTbx2* activity (2). Also, the appearance of murine *Tbx2* was blocked in *Bmp2* null mouse embryos (2). Thus, *Tbx2* expression depended on Bmp signaling through Smad factors, a regulatory paradigm that also guides other modular-restricted genes in the developing heart.

***Tbx2* Directs EC Formation.** *Tbx2* is generally considered to be a transcriptional repressor. For example, *Tbx2*-null embryos have expanded chamber-specific gene expression into the AVC My (3). Also, *Tbx2*-overexpressing transgenic mice and *Tbx20*-null mice, in which *Tbx2* is up-regulated, exhibited decreased expression of several chamber-specific genes and caused hypoplasia of ventricular chamber (4–6, 18, 19). However, *Tbx2* also contains an activation domain (20), and is important for EC formation, because *Tbx2* null mutant embryos exhibited small AVC and defective OFT septation (3). As shown here, *Tbx2* enhanced ECM synthesis from myocardial cells and EMT from endocardial cells. Tbx2 directly bound *Has2* and *Tgfβ2* promoters and increased their transcriptional activities. Tgfβ signaling is crucial

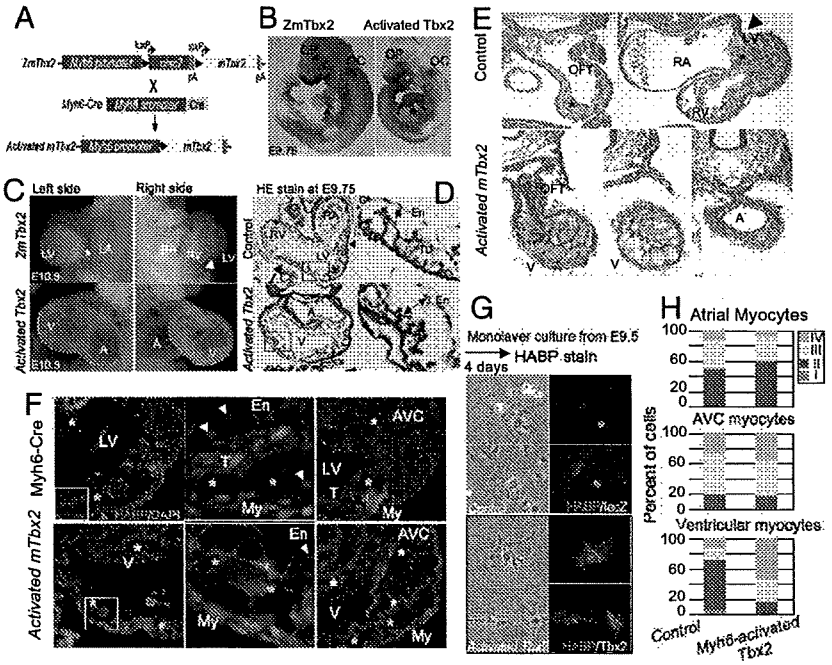

Fig. 3. Abnormal cardiac morphogenesis induced by activated *mTbx2* coincided with excessive HA deposition. (*A*) Schematic representation of *Myh6-Cre* induced activation of *mTbx2* by breeding *ZmTbx2* mice to the Cre deleter mouse line, *Myh6-Cre*. (*B*) Cardiomyocyte-specific activated *mTbx2* was detected by immunoperoxidase staining in the atria and ventricles at E9.75. (*C*) Enlarged images highlight embryonic hearts at E10.5. Relative to control littermates, activated *Tbx2* embryos exhibited an enlarged heart, which appeared as swollen single ventricular and atrial chambers, and a dilated AVC (yellow dotted line in *C*) at E10.5. (*D*) Histological sections of activated *mTbx2* in embryonic hearts at E9.75 stained with HE staining showed rounded ventricular chamber (blue dotted line) and an abnormally narrow ventricular lumen due to expansion of EC like structure between the En and My (two-headed arrow in *D*), and arrow indicate intraventricular sulcus (IVS) and arrowheads indicate AVC. (*E*) Histological sections of embryonic hearts stained at E10.5 with alcian blue revealed acidic glycosaminoglycans (blue stain) not only deposited in the OFT and AVC regions of control littermates (black asterisks), but throughout the chambers of activated *Tbx2* hearts (red asterisks). (*F*) Visualization of HA on sections of E9.75 embryos with HABP (red). HA was deposited between En and My in the inner curvature and AVC of activated *mTbx2* embryos and control littermates (white asterisks) and not in the outer curvature of control littermates. Extra deposition of HA was observed between En and My in the outer curvature of *mTbx2*-misexpressing ventricles (yellow asterisks). DAPI stain was used to visualize nuclei (blue). (*G*) Visualization of HA on cultured ventricular myocytes from embryos of E9.5 or E9.75 with HABP (red). Immunocytochemical detection of lacZ and Tbx2 (green). (*H*) Percentage of classified cardiomyocytes with HA secretion. Type I cardiomyocytes, no secretion of HA; Type II, little amount of HA around the cells; Type III, much HA is secreted around the cells; Type IV, much HA is secreted around the cells and deposited in the cells (Fig. S4). Majority of ventricular cardiomyocytes secreted excessive HA in the activated *mTbx2* embryos. T, trabeculae; CL, compact layer; and TL, trabecular layer.

for EMT in the AV cushions (20–22). Accelerated appearance of EMT from the ventricular and atrial tissues, in vitro EMT assays and increased Smad2 phosphorylation in *mTbx2*-activated embryos supports activation of Tgfβ2 pathway by Tbx2.

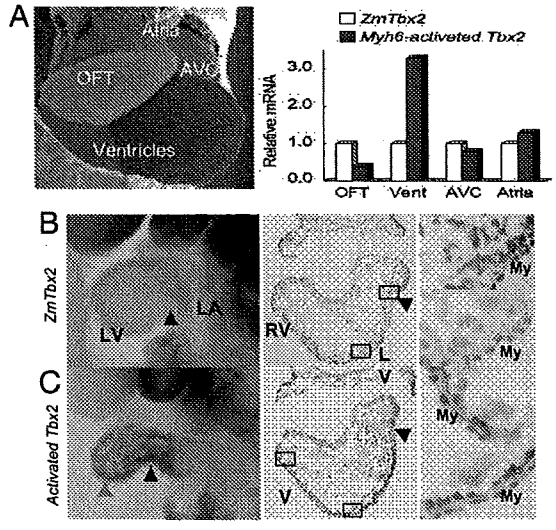

Fig. 4. HA synthetase, *Has2*, activated by *Tbx2* in cardiac chamber myocytes. (*A*) Real-time PCR analysis of dissected embryonic hearts at E9.5 or E9.75. *Has2* transcripts were tripled in the ventricles of activated *mTbx2* embryos. (*B*) Whole-mount in situ hybridization analysis for *Has2* expression was detected in the AVC (black arrowheads) of control littermates whereas expanded to ventricles (red arrowheads) of activated *Tbx2* embryos. The middle and right columns show sections after WISH. *Has2* expression was activated in ventricular myocardial cells of activated *Tbx2* embryos (right column). Nuclear were stained by nuclear fast red.

Tbx2 also induced *Has2* myocardial expression and increased HA deposition. HA is known as an essential factor for EC formation (8, 16, 23), and interacts with other molecules such as versican and fibrillin, which expands cardiac jelly providing extracellular space for cell migration (8). In addition to organizing extracellular environment, HA stimulates EMT of several types of epithelial cells (24) and endocardial cells dependent on Ras-activation (15) via ErbB2 receptor (23). In *Tbx2*-misexpressing embryos, extradeposition of HA was observed in the dilated chamber My; thus, *Tbx2* has an important role in EC formation by increasing synthesis of HA. During normal heart development, chamber-cardiomyocytes undergo a critical maturation step that is manifested by a transition from production to degradation of ECM between E8.0 and E9.5 (25). Whereas HA is required for cushion formation, excess HA deposition may cause hemodynamic alteration and prevent cardiomyocyte differentiation necessary for chamber maturation.

Hierarchical Relationship Between Bmp2/4, *Tbx2*, *Has2*, and *TGFβ2*. We propose a model in which Bmp-Smad responsive *Tbx2* is stimulated to perform a central role in promoting EC formation by inducing expansion of ECM and EMT by directing Has2 and Tgfβ2 gene activity (Fig. 6). Several signaling pathways have been implicated in EC formation. The Bmp pathway is essential for expansion of ECM and EMT in EC formation. Myocardial-specific inactivation of *Bmp2*, *Bmp4*, and a Bmp type I receptor gene, *Alk3*, respectively, failed to form the EC (9, 10, 26). Sugi et al. (11) demonstrated that Bmp2 could substitute for the My to induce EMT. Also, noggin treatment of explants efficiently inhibited EMT. In both chicken and mouse EMT assays, Tgfβ2 is able to replace the overlying My to activate EMT in *Tgfβ2* null mice (11, 16, 21, 22). Analysis of *Tgfβ2*-deficient mice also indicated that Tgfβ2 is important for valvulogenesis (27). Recent studies have shown that several factors, including *Tbx2*, *Tgfβ2*, and *Has2*, are downstream targets of Bmp2/4 pathway (9, 10). In

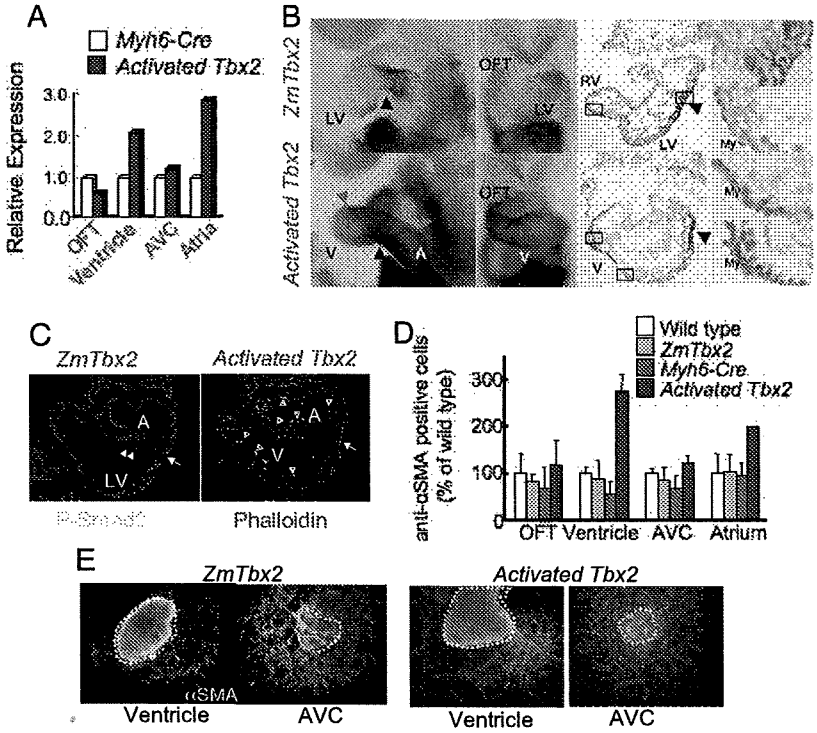

Fig. 5. Activated *mTbx2* induced *Tgfβ2* and enhanced EMT. (*A*) Real-time PCR analysis of quartered embryonic hearts at E9.5. *Tgfβ2* was increased in the ventricles and atria of activated *mTbx2* heart. (*B*) Whole-mount in situ hybridization analysis detected *Tgfβ2* expression in the AVC (black arrowheads in controls) and OFT of control littermates which expanded to ventricles and atria of activated *Tbx2* hearts (red arrowheads in misexpressed *Tbx2*). The middle and right columns show sections after WISH. *Tgfβ2* expression was activated in ventricular myocardial cells of activated *Tbx2* embryos (right column). Nuclear were stained by nuclear fast red. (*C*) Immunohistochemical detection of phospho-Smad2, an effector of Tgfβ signaling in the AVC (white arrows) En of control littermates (white arrowheads), which was expanded to the En of the ventricles and atria in activated *mTbx2* hearts (red arrowheads). (*D* and *E*) Immunohistochemical detection of α-smooth muscle actin (SMA) showed increased EMT in in vitro collagen gel assays of ventricular and atrial explants. The percentage of anti-αSMA positive cells formed in explants from *mTbx2*-misexpressing ventricles and atria was approximately doubled compared with controls.

addition to myocardial-derived Bmp function, Bmp signals directly to the cushion En through the Bmpr1a to induce EMT (9). In our experiments, Bmp2/4 were not up-regulated in *Tbx2*-misexpressing embryos (Fig. S7). Recently, Singh et al. (28) showed that Tbx20 directly interfered with Bmp/Smad signaling to suppress Tbx2 expression in the chambers; thereby, confining Tbx2 expression to the prospective AVC region. They also confirmed our observation that Tbx2 distal enhancer directs Tbx2 expression to the AVC and OFT. Here, we showed Bmp-Smad signaling dependent *Tbx2* expression directed *Has2* and *Tgfβ2* gene activity to coordinately regulate EC formation.

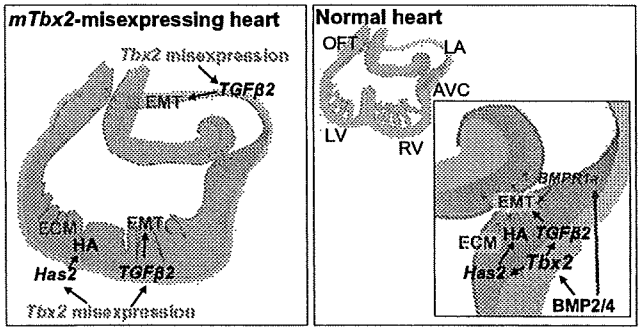

Fig. 6. Model of *Tbx2* function for the EC formation in the AVC. The *mTbx2* misexpression induces expression of *Has2*; thereby, driving the synthesis and deposition of HA and/or cardiac jelly through the heart. Misexpressed *Tbx2* signals also promoted expression of Tgfβ2 gene that supports the induction of EMT in the ventricles and atria. In the normal heart development, *Tbx2* works as one of the important factor to induce expansion of ECM and EMT under the Bmp2/4-Smad signaling pathway. Bmp signals also directly to the En through the Bmpr1a.

Experimental Procedures

Generation of *mTbx2* Reporter Gene Constructions. A genomic fragment that contained the *Tbx2* locus was isolated from a 129SVJ mouse genomic library. A 4.5-kb NotI fragment flanking the 5′ transcription start site and overlapping the first coding exon was cloned into the NotI site of pBluescript-KS for sequencing. The *mTbx2* reporter construct were generated from 4.1 kb of *mTbx2* flanking sequence 5′ was linked in-frame in front of the *lacZ* and luciferase cDNA from pPD46.21 and pGL3-Basic (Promega). Deletion constructs were generated by restriction endonuclease digestion. The region from −2916 to −2602bp, containing multiple Smad sites, was linked to the hsp68lacZ reporter gene (29). Mutations at multiple Smad sites in −2916/−2602 fragment were inserted using In-Fusion PCR cloning kit (Clontech) (Fig. 2*D*; Fig. S1*C*).

Whole-Mount in Situ Hybridization. Staged mouse embryos were obtained after timed mating of mice with the morning of the copulation plug being E0.5. Embryos were fixed in MEMFA (0.1 M Mops/2 mM EGTA/1 mM $MgSO_4$/3.7% formaldehyde) and stored in 90% methanol at −20 °C until use for hybridization. Whole-mount in situ hybridization was performed as described by Yamada et al. (2), except that polyvinyl alcohol was included to increase signal intensity. A full-length of *mTbx2* cDNA (kindly provided by Roni Bollag) was cloned into the *EcoR*I site of pBluescript-KS to synthesize digoxigenin-labeled RNA probes. After restriction endonuclease digestion with SacI, antisense probes were transcribed with RNA labeling kit (Stratagene).

Transient Transfection Assays. Monkey CV-1 fibroblasts were grown in DMEM with 10% FBS. Cells were plated at 1×10^5 cells per well in a 24-well plate and transfected 24 h later with DNA mixture containing a total of 2 μg of total DNA, which included 500 ng of luciferase reporter vector, 500 ng of β-galactosidase vector, and a total of 1 μg of pCMV5-derived vectors. Transfections were performed using Lipofectamine (Invitrogen) as described (30). Luciferase activity were measured using a luminometer to detect activates substrates, then normalized by β-galactosidase activity (29).

Histology. Embryos were dissected in Dulbeco's PBS and fixed overnight at 4 °C in 4% PFA in PBS for histological analysis. After fixation, embryos were rinsed in PBS, then dehydrated through graded ethanol or methanol and embedded in paraffin wax. Sections were cut and stained with hematoxylin-eosin or alcian blue according to standard methods. The HA was detected with 2 μg/mL biotinylated HABP isolated from bovine nasal cartilage (Seikagaku). The HABP was detected using streptavidin-conjugated AlexaFluor (Invitrogen). For immunohistochemistry, sections were incubated with rabbit anti-TBX2 IgG (Upstate Biotechnology) or rabbit anti-β-galactosidase (Biogenesis). Primary antibody was detected with goat anti-rabbit IgG labeled with Alexa Fluor (Invitrogen).

Real-Time PCR. Embryonic hearts at E9.5–E9.75 were divided to 4-parts, OFT, ventricles, AVC, atria at the posterior boundary of EC in OFT, anterior and posterior boundaries of EC. Dissected tissues were immediately frozen in liquid nitrogen and stored at −80 °C until embryo and yolk sac DNA was genotyped. Total RNA isolation and first strand cDNA synthesis were performed with TRIzol reagent, SuperScript III (Invitrogen) and random primer, as per the manufacturer's instructions.

Primary Culture of Embryonic Cardiac Cells and Classification of Cardiomyocytes with HA Synthesis. Quartered embryonic cardiac tissues were separated as described above. After trypsinization, isolated cardiac cells were cultured on gelatinized dishes by using culture medium containing DMEM (D5796; Sigma–Aldrich), 10% heat-inactivated FCS (HyClone), 0.1 g/mL penicillin, and 0.1 mg/mL streptomycin. After 4 days culture, cells were fixed in 4% PFA in PBS and detected HA, Tbx2 and β-galactosidase as described above. Classification of cardiomyocytes with HA secretion was followed as described in Fig. S4.

1. Schwartz RJ, Olson EN (1999) Building the heart piece by piece: Modularity of *cis*-elements regulating to Nkx2–5 transcription. *Development* 126:4187–4192.
2. Yamada M, et al. (2000) Expression Of Chick Tbx-2, Tbx-3 and Tbx-5 genes during early heart development: Evidence for BMP2 induction of Tbx2. *Dev Biol* 228:95–105.
3. Harrelson Z, et al. (2004) Tbx2 is essential for patterning the atrioventricular canal and for morphogenesis of the outflow tract during heart development. *Development* 131:5041–5052.
4. Christoffels VM, et al. (2004) T-box transcription factor Tbx2 represses differentiation and formation of the cardiac chambers. *Devl Dyn* 229:763–770.
5. Habets PE, et al. (2002) Cooperative action of Tbx2 and Nkx2.5 inhibits ANF expression in the atrioventricular canal: Implications for cardiac chamber formation. *Genes Dev* 16:1234–1246.
6. Cai CL, et al. (2005) T-box genes coordinate regional rates of proliferation and regional specification during cardiogenesis. *Development* 132:2475–2487.
7. Pierpont ME, Markwald RR, Lin AE (2001) Genetic aspects of atrioventricular septal defects. *Am J Med Genet* 297:289–296.
8. Schroeder JA, Jackson LF, Lee DC, Camenisch TD (2003) Form and function of developing heart valves: Coordination by extracellular matrix and growth factor signaling. *J Mol Med* 81:392–403.
9. Ma L, Lu MF, Schwartz RJ, Martin JF (2005) Bmp2 is essential for cardiac cushion epithelial-mesenchymal transition and myocardial patterning. *Development* 132:5601–5611.
10. Gaussin V, et al. (2002) Endocardial cushion and myocardial defects after cardiac myocyte-specific conditional deletion of the bone morphogenetic protein receptor ALK3. *Proc Natl Acad Sci USA* 99:2878–2883.
11. Sugi Y, Yamamura H, Okagawa H, Markwald RR (2004) Bone morphogenetic protein-2 can mediate myocardial regulation of atrioventricular cushion mesenchymal cell formation in mice. *Dev Biol* 269:505–518.
12. Itoh S, Itoh F, Goumans MJ, Ten Dijke P (2000) Signaling of transforming growth factor-beta family members through Smad proteins. *Eur J Biochem* 267:6954–6967.
13. Galvin KM, et al. (2000) A role for smad6 in development and homeostasis of the cardiovascular system. *Nat Genet* 24:171–174.
14. Yamada M, et al. (1999) Evidence for a role of Smad6 in chick cardiac development. *Dev Biol* 215:48–61.
15. Whiteman P (1973) The quantitative measurement of Alcian Blue glycosaminoglycan complexes. *Biochem J* 131:343–350.
16. Camenisch TD, et al. (2000) Disruption of hyaluronan synthase-2 abrogates normal cardiac morphogenesis and hyaluronan-mediated transformation of epithelium to mesenchyme. *J Clin Invest* 106:349–360.
17. Baldwin HS, Lloyd TR, Solursh M (1994) Hyaluronate degradation affects ventricular function of the early postlooped embryonic rat heart in situ. *Circ Res* 74:244–252.
18. Stennard FA, Harvey RP (2005) T-box transcription factors and their roles in regulatory hierarchies in the developing heart. *Development* 132:4897–4910.
19. Takeuchi JK, et al. (2005) Tbx20 dose-dependently regulates transcription factor networks required for mouse heart and motoneuron development. *Development* 132:2463–2474.
20. Paxton C, Zhao H, Chin Y, Langner K, Reecy J (2002) Murine Tbx2 contains domains that activate and repress gene transcription. *Gene* 283:117–124.
21. Brown CB, Boyer AS, Runyan RB, Barnett JV (1999) Requirement of type III TGF-beta receptor for endocardial cell transformation in the heart. *Science* 283:2080–2082.
22. Nakajima Y, Yamagishi T, Hokari S, Nakamura H (2000) Mechanisms involved in valvuloseptal endocardial cushion formation in early cardiogenesis: Roles of transforming growth factor (TGF)-beta and bone morphogenetic protein (BMP). *Anat Rec* 258:119–127.
23. Camenisch TD, Schroeder JA, Bradley J, Klewer SE, McDonald JA (2002) Heart-valve mesenchyme formation is dependent on hyaluronan-augmented activation of ErbB2-ErbB3 receptors. *Nat Med* 8:850–855.
24. Zoltan-Jones A, Huang L, Ghatak S, Toole BP (2003) Elevated hyaluronan production induces mesenchymal and transformed properties in epithelial cells. *J Biol Chem* 278:45801–45810.
25. Bernanke DH, Orkin RW (1984) Hyaluronidase activity in embryonic chick heart muscle and cushion tissue and cells. *Dev Biology* 106:351–359.
26. Jiao K, et al. (2003) An essential role of Bmp4 in the atrioventricular septation of the mouse heart. *Genes Dev* 17:2362–2367.
27. Bartram U, et al. (2001) Double-outlet right ventricle and overriding tricuspid valve reflect disturbances of looping, myocardialization, endocardial cushion differentiation, and apoptosis in TGF-beta (2)-knockout mice. *Circulation* 103:2745–2752.
28. Singh R, et al. (2009) Tbx20 interacts with smads to confine tbx2 expression to the atrioventricular canal. *Circ Res* 105:442–452.
29. Chi X, et al. (2005) Complex cardiac Nkx2–5 gene expression activated by noggin-sensitive enhancers followed by chamber-specific modules. *Proc Natl Acad Sci USA* 102:13490–13495.
30. Brown CO, III, et al. (2004) The cardiac determination factor, Nkx2–5, is activated by mutual cofactors GATA-4 and Smad1/4 via a novel upstream enhancer. *J Biol Chem* 279:10659–10669.

RNA-binding proteins Rbm38 and Rbm24 regulate myogenic differentiation via p21-dependent and -independent regulatory pathways

Shoko Miyamoto[1,2], Kyoko Hidaka[1], Donghao Jin[1] and Takayuki Morisaki[1,2]*

[1]*Department of Bioscience, National Cardiovascular Center Research Institute, Suita, Osaka 565-8565, Japan*
[2]*Department of Molecular Pathophysiology, Osaka University Graduate School of Pharmaceutical Sciences, Suita, Osaka 565-8565, Japan*

Skeletal muscle differentiation entails organized sequential events, including cell cycle arrest of proliferating myoblast cells and cell fusion, which lead to the formation of multinucleated myotubes. This process involves both transcriptional and post-transcriptional regulation of the gene expression of myogenic proteins, as well as cell-cycle related proteins. RNA-binding proteins bind to specific sequences of target RNA and regulate gene expression in a post-transcriptional manner. However, few tissue-specific RNA binding proteins have been identified. Herein, we report that the RNA binding proteins Rbm24 and Rbm38 were found to be preferentially expressed in muscle during differentiation *in vitro*. Further, knockdown of either by RNA interference suppressed cell-cycle arrest and delayed myogenic differentiation in C2C12 cells. In contrast, over-expression of Rbm24 or Rbm38 induced cell cycle arrest, and then had a positive effect on myogenic differentiation. Immunoprecipitation-RT-PCR analysis using tagged Rbm proteins indicated that Rbm38 binds to the p21 transcript *in vivo*. Consistent with this, differentiation of Rbm38 knockdown cells was rescued by over-expression of p21. Together, our results suggest that Rbm38 plays a crucial role in cell cycle arrest and myogenic differentiation via its binding to p21.

Introduction

In myogenic differentiation, proliferating myoblasts first exit from the cell cycle and are fused to form multinucleated myotubes with a contractile phenotype and then myofibers. These transition steps are known to be controlled by myogenic regulatory factors (MRFs), such as MyoD, Myf5, myogenin and MRF4. Indeed, muscle progenitor cells remain undifferentiated in independent myogenic compartments during embryonic development when these MRFs are missing (Kablar *et al.* 2003). It is known that MRFs and p21cip1 (p21), a cyclin-dependent kinase inhibitor, coregulate each other, and that p21 inhibits the activity of cyclin/cdk2 complexes and regulates mammalian cell cycle arrest (el-Deiry *et al.* 1993, 1994; Brugarolas *et al.* 1999), which is essential for myogenic differentiation. MyoD also activates p21 and induces the withdrawal of myoblasts from the cell cycle, an integral part of myogenic differentiation (Sorrentino *et al.* 1990; Guo *et al.* 1995). In myogenic cells, p21 is increasingly expressed during the G1 phase of the cell cycle, although a high level is required for myotube maintenance (Odelberg *et al.* 2000), while p21 induces myogenin expression during the myoblast-to-myotube transition (Halevy *et al.* 1995). Therefore, skeletal muscle differentiation entails the coordination of MRFs and terminal withdrawal from the cell cycle. Early studies using cultured myoblasts showed that cell-cycle exit and differentiation are coupled (Bischoff & Holtzer 1969; Nadal-Ginard 1978; Clegg *et al.* 1987). Mice lacking p21 undergo normal development, but are defective in G1 checkpoint control (Deng *et al.* 1995). Mice lacking both Cdk inhibitors, p21 and p57, display

Communicated by: Fumio Hanaoka
**Correspondence*: morisaki@ri.ncvc.go.jp

DOI: 10.1111/j.1365-2443.2009.01347.x

severe skeletal muscle defects, manifested as a failure to form myotubes, with increased proliferation of myoblasts (Zhang *et al.* 1999). However, the molecules controlling cell-cycle exit and the differentiation steps dependent on cell-cycle arrest are poorly understood.

In addition to transcriptional regulation, post-transcriptional regulation of muscle-specific genes has important roles in myogenesis. RNA-binding proteins are known to regulate gene expression in a post-transcriptional manner, such as for RNA splicing, transport, stability, polyadenylation and translation (Krecic & Swanson 1999), which have recently been noted to be critical mechanisms for gene regulation in mammalian cells. For example, HuR, which contains the RNA recognition motif (RRM), is known to be associated with the AU-rich element (ARE) in the 3′-UTR of MyoD, myogenin and p21 mRNA, and also contributes to the progression of myogenesis by stabilizing mRNA (Wang *et al.* 2000; Figueroa *et al.* 2003). Another RNA binding protein, NF90, containing two double-stranded RNA-binding domains, is also associated with and stabilizes the mRNA of its targets, MyoD and p21, by binding to the ARE in the 3′-UTR in developing muscle (Shim *et al.* 2002). However, expression of these RNA binding proteins is not muscle-specific, as HuR is also expressed in intestinal epithelial cells, where it modulates the stability of its target, activating transcription factor-2 (ATF-2) mRNA(Xiao *et al.* 2007). NF90 is also strongly expressed in testis and brain tissues, although it has moderate expression in the heart, spleen, lungs, liver and kidneys (Shi *et al.* 2005). Therefore, muscle-specific RNA binding proteins have never been reported in mammals and their mechanisms of post-transcriptional regulation during myogenesis remain unclear.

Previously, we identified several genes that are specifically expressed during the course of cell differentiation of ES cells using DNA microarray analysis (Terami *et al.* 2007), with Rbm24 shown to be one of these genes. A homology search with the deduced amino acid sequences showed that the Rbm24 gene product shares a significant similarity with that of Rbm38, suggesting that these genes are paralogues. A previous study showed that the *Caenorhabditis elegans* homologue of these genes, sup12, specifically regulated expression of a muscle-specific gene during myogenic development (Anyanful *et al.* 2004). Furthermore, human Rbm38 (also known as RNPC1) was previously investigated using a human colorectal cancer cell line and shown to induce cell cycle arrest in the G1 phase by regulating the stability of p21 mRNA. In the present study, we showed that Rbm24 and Rbm38 are RNA-binding proteins preferentially expressed in cardiac and skeletal muscle tissues, and then investigated the functions of these proteins for myogenesis, and found that both regulate myogenic differentiation by controlling the cell cycle in a p21-dependent or -independent manner.

Results

Expressions of Rbm24 and Rbm38 in cardiac and skeletal muscle tissues

We selected several genes specifically expressed during cell differentiation of multipotential ES cells using DNA microarray analysis (Terami *et al.* 2007) and considered them as candidate genes that function in cell differentiation processes for the present experiments. Rbm24, found to be increasingly expressed during cardiomyocyte differentiation, was selected as one of these candidate genes. This gene is an RNA binding protein that contains an RRM, which is the most prevalent type of eukaryotic RNA-binding motif (Dreyfuss *et al.* 1993). In addition, Rbm38 was also selected, because it is the paralogue of Rbm24. To investigate the expression profiles of Rbm24 and Rbm38, QRT-PCR analysis was carried out using various organs and tissues from adult mice (Fig. 1A,B). Consistent with the muscle-tissue specific expression of sup12 in *C. elegans*, both Rbm24 and Rbm38 were found to be preferentially expressed in cardiac and skeletal muscle tissues. Furthermore, we monitored the expression profiles of Rbm24 and Rbm38 during the course of myogenic differentiation of C2C12 myoblast cells (Yamaguchi 1995) using QRT-PCR analysis (Fig. 1C–F), which showed that their mRNA expression increased when the myoblast-to-myotube transition occurred in those cells.

Knockdown of Rbm24 and Rbm38 inhibits myogenic differentiation

To investigate whether Rbm24 and Rbm38 play roles in myogenic differentiation, a gene knockdown experiment was conducted using an RNAi method. C2C12 myoblast cells at 100% confluence were transfected with an siRNA duplex for Rbm24 or Rbm38, then differentiation was immediately induced by changing to differentiation medium (Fig. 2A). A non-specific siRNA duplex was also used as the control

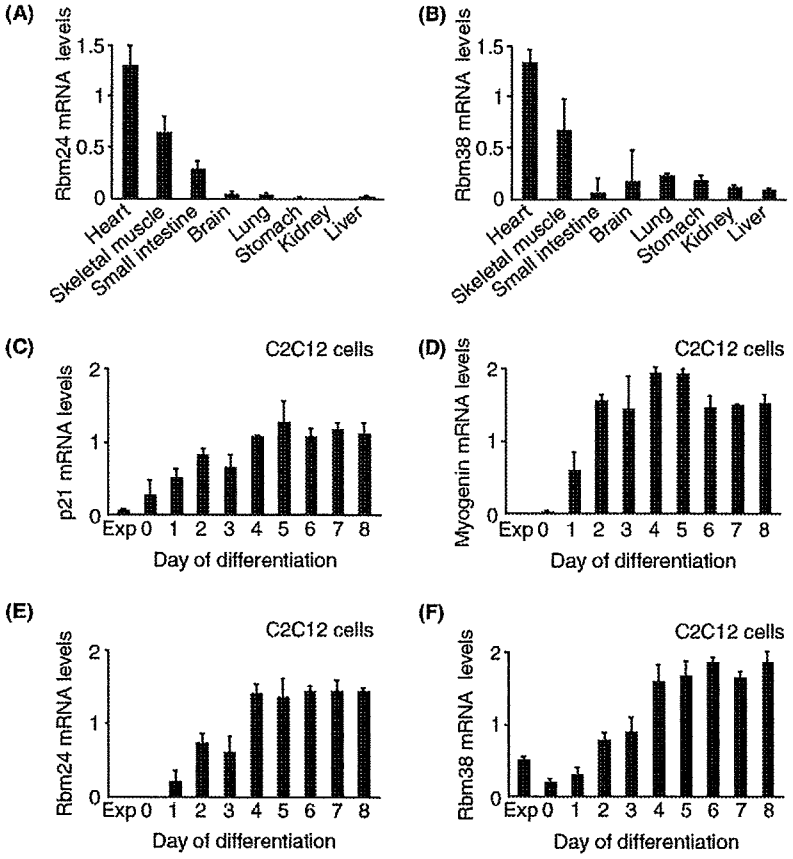

Figure 1 Preferential expressions of Rbm24 and Rbm38, RNA binding proteins, during myogenesis. (A, B) QRT-PCR analyses were carried out using various organs and tissues from adult mice. RNA was reverse-transcribed and then PCR-amplified using Rbm24- or Rbm38-specific primers. Both Rbm24 and Rbm38 were preferentially expressed in muscle tissues. (C, D) QRT-PCR was carried out during the course of myogenic differentiation of C2C12 myoblast cells to detect p21 and myogenin. Expressions of p21 and myogenin were highly maintained in differentiating C2C12 cells. (E, F) QRT-PCR was carried out to detect Rbm24 and Rbm38. The expressions of Rbm24 and Rbm38 were increased in differentiating C2C12 cells. Error bars indicate the standard error. Values shown are the average of three experiments.

siRNA to verify the specificity of the experiments. The inhibitory effects of the siRNA duplexes were examined by QRT-PCR. On day 2 of differentiation, the mRNA levels of Rbm24 and Rbm38 were decreased by more than 80% by transfection with Rbm24 siRNA and Rbm38 siRNA, respectively, as compared with the control siRNA. Next, to assess the effects of their decreased expression on myogenic differentiation, immunofluorescence staining for myosin heavy chain (MyHC) was carried out to check myotube formation on day 4 of differentiation (Fig. 2B,C). We found that MyHC-positive myotubes were significantly decreased in cells transfected with Rbm24 and Rbm38 siRNA as compared with those transfected with the control siRNA. These results suggest that Rbm24 and Rbm38 play important roles in myotube formation during myogenic differentiation.

The first step of myogenic differentiation in a model such as C2C12 cells is the cell cycle arrest of myoblasts, followed by cell fusion and multinucleated myotube formation. As human Rbm38 (RNPC1) is known to induce cell cycle arrest in the G1 phase of RKO cells, a human colorectal cancer cell line (Shu *et al.* 2006), we next investigated whether inhibition of Rbm24 and Rbm38 would affect DNA synthesis or mitosis by performing immunofluorescence staining with the anti-5-bromodeoxyuridine (BrdU) antibody, a marker of DNA synthesis, and the anti-phosphorylated histone H3 (phospho-HH3) antibody,

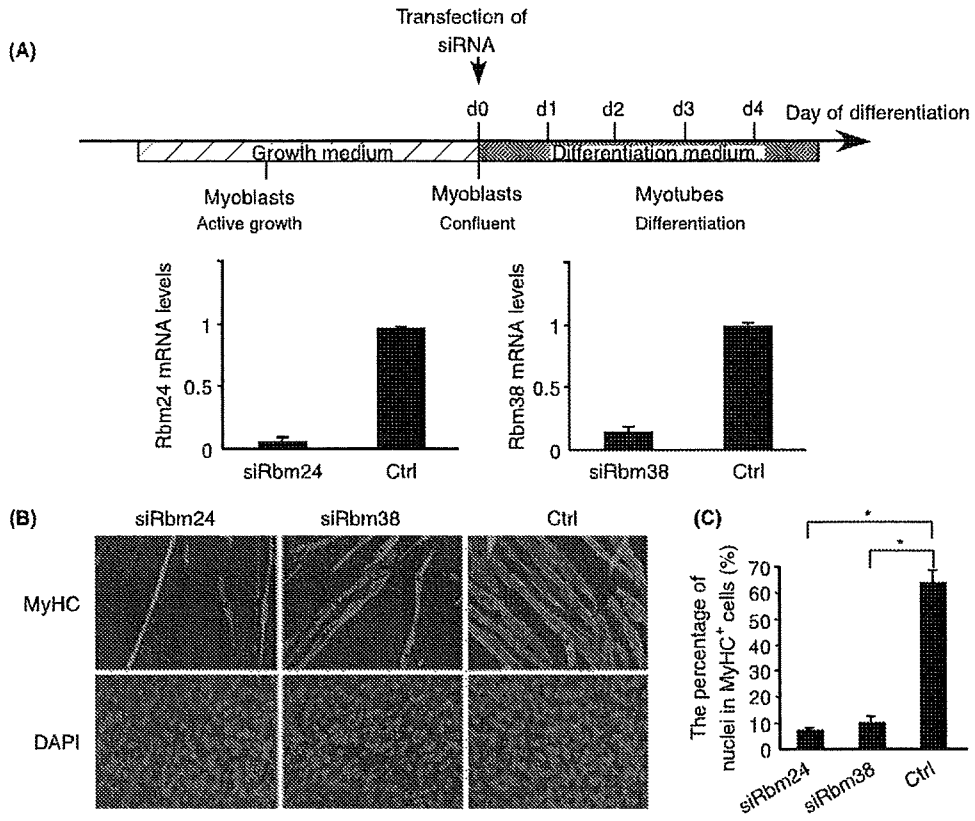

Figure 2 Knockdown of Rbm24 and Rbm38 inhibits myotube formation during C2C12 differentiation. (A) Schematic diagram of siRNA transfection protocol during C2C12 cell differentiation. C2C12 cells at 100% confluence were transfected with Rbm24 or Rbm38 siRNA on the day of differentiation induction. The inhibitory effects of siRNA duplexes were examined on day 2 by QRT-PCR. Error bars indicate the standard error. Values shown are the average of three experiments. (B) C2C12 cells were treated with siRNA on the day of differentiation and fixed on day 4. Cells were stained with anti-MyHC antibody and DAPI to determine their differentiation status. When cells were transfected with the Rbm24 or Rbm38 siRNA duplex, the number of MyHC-positive myotubes was significantly decreased as compared with the control siRNA. (C) The percentage of nuclei in MyHC-positive cells was calculated to assess differentiation efficiency of C2C12 cells treated with siRbm24 or siRbm38. Error bars indicate the standard error. Values shown are the average of three experiments ($*P < 0.005$). siRbm24, Rbm24 siRNA duplex; siRbm38, Rbm38 siRNA duplex; Ctrl, control siRNA duplex.

a marker of mitosis, on day 4 of differentiation (Fig. 3A,B). When the cells were transfected with Rbm38 siRNA, BrdU-positive and phospho-HH3-positive cells were increased by 180% and 110%, respectively, as compared with the control siRNA (Fig. 3C). When transfected with Rbm24 siRNA, BrdU-positive and phospho-HH3-positive cells were increased by 167% and 70%, respectively (Fig. 3C). By prolonging the BrdU incorporation time (24 hours), the percentage of BrdU-positive nuclei increased (17% of total nuclei in Rbm24-knockdown and 16% in Rbm38-knockdown cultures). However, we did not observe a robust increase in numbers of proliferating cells (data not shown). These results suggest that knockdown of Rbm24 and Rbm38 suppresses cell cycle arrest and delays myogenic differentiation, although their effects on cell cycles remain to be determined.

Over-expression of Rbm24 and Rbm38 promotes myogenic differentiation

To further investigate whether Rbm24 and Rbm38 have effects on myogenic differentiation, an experiment was employed utilizing their over-expression. To increase transfection efficiency, plasmids were introduced 1 day before differentiation induction, when the cells had reached 70%–80% confluence.